High-dose, intermediate-temperature neutron irradiation effects on silicon carbide composites with varied fiber/matrix interfaces*

Takashi Nozawa[1], Takaaki Koyanagi[2], Yutai Katoh[2], Hiroyasu Tanigawa[1]

[1]*National Institutes for Quantum and Radiological Science and Technology (QST), Rokkasho, Aomori, 039-3212 Japan*

[2]*Oak Ridge National Laboratory (ORNL), Oak Ridge, TN 37831 USA*

Abstract

SiC/SiC composites are promising structural candidate materials for various nuclear applications over the wide temperature range of 300–1000°C. Accordingly, irradiation tolerance over this wide temperature range needs to be understood to ensure the performance of these composites. In this study, neutron irradiation effects on dimensional stability and mechanical properties to high doses (11–44 dpa) at intermediate irradiation temperatures (~600°C) were evaluated for Hi-Nicalon Type-S or Tyranno-SA3 fiber–reinforced SiC matrix composites produced by chemical vapor infiltration. The influence of various fiber/matrix interfaces, such as a 50–120 nm thick pyrolytic carbon (PyC) monolayer interphase and 70–130 nm thick PyC with a subsequent PyC (~20 nm)/SiC (~100 nm) multilayer, was evaluated and compared with the previous results for a thin-layer PyC (~20 nm)/SiC (~100 nm) multilayer interphase. Four-point flexural tests were conducted to evaluate post-irradiation strength, and SEM and TEM were used to investigate microstructure. Regardless of the fiber type, monolayer composites showed considerable reduction of flexural properties after irradiation to 11–12 dpa at 450–500°C; and neither type showed the deterioration identified at the same dose level at higher temperatures (>750°C) in a previous study. After further irradiation to 44 dpa at 590–640°C, the degradation was enhanced compared with conventional multilayer composites with a PyC thickness of ~20 nm. Multilayer composites have shown comparatively good strength retention for irradiation to ~40 dpa, with moderate mechanical property degradation beginning at 70–100 dpa. Irradiation-induced debonding at the F/M interface was found to be the major cause of deterioration of various composites.

Key words: Silicon carbide fiber-reinforced silicon carbide matrix composites, neutron irradiation, intermediate temperature, fiber/matrix interface, flexural properties

Introduction

Silicon carbide (SiC) possesses advantageous features as a nuclear material, including superior mechanical properties at elevated temperatures, good chemical inertness, low activation and low decay-heat, and perceived radiation tolerance [1–3]. Continuous SiC-fiber–reinforced, SiC matrix (SiC/SiC) composites are generally considered for practical applications because monolithic SiC is brittle, making it very difficult for it to comply with many structural requirements. Therefore, SiC/SiC composites are now being considered in a wide variety of nuclear fields for various application temperature ranges: full SiC/SiC composite blankets (~1000°C) [4] and flow channel inserts as functional structures of dual-coolant lithium lead blankets (600–700°C) [5–8] for fusion DEMO applications, control rods for very-high-temperature fission reactors and gas-cooled fast reactors (800–1000°C) [9–11], and accident-tolerant fuel cladding and channel boxes for light water reactors (~300°C) [12–14]. Structural SiC/SiC composites must maintain their integrity not only in normal operation but also under accidental conditions at elevated temperatures (mostly above 1200°C, depending on the accident scenario [15–17]). Accordingly, irradiation tolerance over a wide temperature range needs to be understood to ensure the performance of SiC/SiC composites because high-energy neutron irradiation bombardment introduces lattice defects that result in property changes.

Irradiation studies begun in the middle 1970s to develop protective nuclear fuel coatings [18] and were extended to other nuclear structural applications. One notable breakthrough in the research history of SiC/SiC composites was the innovation of highly crystalline and near-stoichiometric radiation-tolerant SiC fibers, e.g., Hi-Nicalon Type-S (HNS) [19], Tyranno-SA3 (SA3) [20], and Sylramic [21]. Because they are more radiation tolerant, these fibers have superior strength retention during neutron irradiation [22, 23]. Following this remarkable achievement, research and development in SiC/SiC composites have accelerated in the past decade. For instance, first, the excellent fracture resistance of SiC/SiC composites was demonstrated [24]. Resistance to irradiation degradation at very high temperatures (~1300°C) was proved [25, 26]. Now, the capabilities of new technologies, e.g., the nano-infiltration transient eutectic (NITE) process for robust composite production [27] and various types of joining technologies [28], are being demonstrated.

The fiber/matrix (F/M) interface plays a major role in giving these composites quasi-ductility [29, 30]. Boron nitride, one of the major interface options for SiC/SiC composites, has been widely adopted as an anti-oxidation barrier in aerospace applications [30, 31]; but it is not highly compatible with nuclear applications because neutron irradiation can produce undesirable helium bubbles due to the nuclear transmutation of boron. Alternatively, pyrolytic carbon (PyC) is generally considered as a F/M interface material for nuclear applications. However, the stability of the PyC interphase in neutron irradiation environments must be investigated. Irradiation-induced swelling and modification of the mechanical

properties of PyC greatly affect the residual stress at the F/M interphase [32], which influences its mechanical properties. Irradiation effects on PyC must be identified along with the effects on SiC.

Understanding irradiation effects on the F/M interface is challenging because the PyC microstructure depends on the processing conditions, and the effects of irradiation on carbon are known to vary with the initial microstructure. Kaae et al. summarized the irradiation behavior of isotropic PyC, i.e., turbostratic graphitic structure [33–37]. Isotropic PyC first shows shrinkage in the direction perpendicular to the deposition plane after irradiation to a few displacements per atom (dpa), followed by swelling up to at most 10 dpa, depending on density called "turn around behavior." In contrast, shrinkage in the direction parallel to the deposition plane was found to continue at higher neutron doses. It was also reported that the elastic modulus of isotropic PyC tended to monotonically increase with increasing neutron dose; it was more than doubled after irradiation to a neutron fluence of ~8×10^{25} n/m^2 (E > 0.18 MeV). Virgil'ev et al. [38] also evaluated the effects of irradiation on glassy carbon, which has a globular-cellular microstructure with turbostratic carbon. It showed a very similar trend to low-density isotropic PyC. In this case, no secondary swelling was reported for irradiation to ~4×10^{26} n/m^2 (E > 0.18 MeV). Similarly, saturation of the elastic modulus at higher doses was found up to a neutron dose >1×10^{21} n/m^2. In addition, recent studies found microstructural instabilities of the PyC interphase under high-dose irradiation environments, as explained below.

In the past decade, continuous efforts have been devoted to the study of a specific type of chemical-vapor-infiltrated (CVI) SiC/SiC composite, with multilayer PyC/SiC interface-coated HNS SiC fibers, irradiated up to ~100 dpa in the High Flux Isotope Reactor (HFIR) at Oak Ridge National Laboratory [39–42]. The key findings are the temperature-dependent response of the SiC/SiC composite to irradiation: (1) retention or slight degradation of the mechanical properties following irradiation up to 70 dpa at ~800°C with moderate fiber pullout; (2) considerable mechanical degradation to 100 dpa at ~600°C with progressive fiber pullout by partial interfacial debonding; and (3) severe degradation to 100 dpa at ~300°C showing brittle fracture with no fiber pullout, associated with significant radiation-induced debonding at the F/M interface. Material degradation was obvious after high-dose irradiation at relatively low temperatures for composites with a multilayer interface, but previous results show that a multilayer interface with thin-layered PyC is viable for nuclear applications in high irradiation temperatures.

Monolayer PyC is another promising option for the F/M interface of SiC/SiC composites because of the simplicity of the structure. Similar to the results for multilayer composites, the stability of the mechanical properties of monolayer composites under irradiation to a few dpa was demonstrated [26]. However, fundamental knowledge of the irradiation effects on monolayer interface composites is still limited in order to have an optimized PyC interlayer. In particular, no data are currently available for neutron irradiation beyond 12 dpa. This study thus aims to investigate the effects of neutron irradiation on

the dimensional stability and mechanical properties of monolayer composites to higher doses (11–44 dpa) at intermediate irradiation temperatures (~600°C). In addition, this paper reports on the high-dose irradiation resistance of SiC/SiC composites made with SA3 fibers, which is also insufficiently studied.

Experimental

Several SiC/SiC composite plates used for the irradiation study were fabricated by Hyper-Therm High-Temperature Composites Inc. (presently Rolls Royce High-Temperature Composites Inc.). The key specifications of the materials are listed in Table 1. The reinforcing SiC fibers were third-generation highly crystalline and near-stoichiometric SiC fibers, i.e., HNS and SA3. Plain-weave and satin-weave architectures were adopted, depending on the material types. The SiC matrix was formed via CVI for all composites. In this study, two different types of the F/M interface were applied (e.g., monolayer or multilayer); but the innermost PyC interlayer formed over the SiC fibers had almost the same characteristics; a single 50–130 nm-thick PyC layer was formed regardless of the interface type (Fig. 1). Subsequent PyC/SiC sub-layers of multilayer composites were formed with an original intention to provide not only resistance against environmental attacks, e.g., oxidation [43], but also more crack resistance, e.g., enhanced deflection of micro cracks at the interface [31]. In a configuration similar to previous multilayer composites [39–42], very thin (~20 nm) PyC sub-layers were formed with 100 nm thick SiC separations. Note that the innermost PyC layer of previous multilayer composites was thinner (~20 nm) than that of the multilayer composite materials tested in this study. Both the PyC and SiC interlayers were formed in the same CVI furnace before the SiC matrix was densified. The density and the porosity were approximately 2.41–2.56 g/cm^3 and 18–22%, respectively. Hereinafter, HNS-fiber–reinforced CVI-SiC matrix composites with a PyC monolayer and those with a PyC/SiC multilayer are denoted as HNS-C and HNS-C/ML, respectively. In a similar manner, SA3-fiber–reinforced CVI-SiC matrix composites with a monolayer and with a multilayer are denoted as SA3-C and SA3-C/ML, respectively. The thin-layer multilayer composites in previous studies [39–42] are hereinafter referred to as HNS-ML.

Neutron irradiation in the HFIR used rabbit-type capsules. A total of 20 miniature flexural specimens (5 for each material type) with dimensions of 25×2.8×1 mm were contained in each capsule. The longitudinal direction was parallel to the reinforcing fibers. The neutron doses were determined to be 11, 12, and 44 dpa for radiation capsules numbered JCR11-06, JCR11-02, and JCR11-01, respectively. The conversion assumed that 1 dpa corresponds to 1.0×10^{25} n/m^2 (E > 0.1 MeV) for SiC, as in the previous study [42]. The irradiation temperatures were obtained from the SiC passive temperature monitors, indicating 500°C (JCR11-06), 450°C (JCR11-02), and 590–640°C (JCR11-01). Note that thermal recovery of expansion by isochronal annealing was used to determine the irradiation temperature, as

explained in [44]. The good agreement in irradiation temperatures measured by dilatometry and other methods such as resistivity was demonstrated, and the typical precision of the analysis was reportedly 10–15°C [44].

Dimensional inspection of the irradiated specimens was used to evaluate swelling of the SiC/SiC composite bars. All dimensions were measured by micrometer with a precision of ±0.001 mm. The dynamic Young's moduli were determined by the nondestructive impulse excitation of the vibration method in accordance with ASTM C1259. Post-irradiation mechanical properties were evaluated by the miniature four-point flexural test method at room temperature in ambient air by referring to ASTM C1341. The loading and support spans of the fixture were 10 and 20 mm, respectively, and the crosshead speed was 0.5 mm/min. The tangent flexural modulus was determined from the slope in the initial linear segment of the flexural stress vs. apparent strain curve. Note that the flexural strain was calculated from the crosshead displacement. The proportional limit stress (PLS) was determined as a 5% deviation in stress from the initial linearity, and the ultimate flexural strength (UFS) was identified as the peak stress. After mechanical tests, fracture surfaces were examined in an FEI Versa Dual Beam scanning electron microscope (SEM)/focused ion beam (FIB), and cross-sections were examined in a JEOL JEM2100F with transmission electron microscopy (TEM) and scanning TEM (STEM) modes operated at 200 kV.

Results

(1) Swelling

Table 2 summarizes the irradiation-induced dimensional changes in a longitudinal direction, i.e., the length increase, of the rectangular specimens of SiC/SiC composites with varied F/M interfaces irradiated to 11–44 dpa. Figure 2 summarizes the length increase of the CVI SiC/SiC composites, including data obtained in this study and in previous studies [25, 39, 41, 42]. In Figure 2, calculated results from the proposed prediction model [45] are also plotted. The model was empirically obtained from the experimental data in the irradiation temperature range of 220–440°C, but it was suggested that this model could be applied to the higher irradiation temperature regime, to a limit of 800°C. Below the irradiation temperature of 800°C, the length of the CVI SiC/SiC composites tended to increase by less with increasing irradiation temperature, showing good agreement with the model prediction [45]. It was shown that the length increase of the CVI SiC/SiC composites tended to decrease with irradiation temperature for the irradiation case of 44 dpa at 590–640°C. However, this change was not significant compared with the large scatter in the case of irradiation to 44 dpa. Figure 2 shows that the experimental length increase data were bounded by the model prediction in the temperature range of 400–700°C under the irradiation temperatures indicated by the temperature monitors (450–640°C).

(2) Mechanical properties

Figure 3 shows typical flexural stress vs. flexural strain curves for non-irradiated and neutron-irradiated SiC/SiC composites. Note that rapid stress increases beyond a flexural strain of 1% were mainly due to specimen contact with the test fixture. Table 2 also summarizes the flexural strength data, as well as dynamic Young's moduli measured by impulse excitation and the tangent moduli measured in flexural tests. All composite types exhibited severe mechanical degradation due to irradiation. More than a 30% reduction in elastic moduli was identified for all irradiation cases and all material types tested in this study, regardless of the measurement method. The initial tangent moduli clearly decreased, as did the dynamic Young's moduli. Note that the dynamic Young's moduli were, without exception, greater than the flexural tangent moduli, because the flexural strain was calculated from the crosshead displacement and hence the strain is apparent. The PLS reduction was more pronounced; the PLS following irradiation was 13–51% of the non-irradiated values, and nonlinear behavior was initiated at stress levels below 100 MPa in most cases. Similarly, irradiation-induced UFS reduction was obvious in all composite types, even considering HNS specimens that made contact with the fixture. Note that PLS and UFS reductions were especially significant for the HNS composites (HNS-C and HNS-C/ML) after irradiation to the highest neutron dose, i.e., 44 dpa, whereas such mechanical deterioration was comparatively moderate for SA3 composites (SA3-C and SA3-C/ML).

Figure 4 summarizes the dose dependence of the elastic moduli of SiC/SiC composites. Of the modulus data determined by two different evaluation methods, the dynamic Young's modulus data were selected in this plot, except that flexural tangent modulus data in [42] were taken because no dynamic Young's modulus data were measured. The test data for SiC/SiC composites with a thick (>50 nm) innermost PyC layer and a subsequent thin-layer SiC/PyC—i.e., HNS-C/ML and SA3-C/ML in this study—were plotted together with the monolayer composites because the mechanical properties of composites are readily affected by the structure and condition of the innermost PyC layer. In short, the monolayer and the multilayer, both of which have the similar type and thickness of the inner PyC layers, can be plotted together since the inner PyC layer dominates that the mechanical properties. For instance, the matrix cracking deflects at the interface between the fiber and the first PyC layer on the fiber [32]. Indeed, matrix cracking occurred in the F/PyC interface, as shown in the following section. Figure 4 indicates an approximately 40% reduction in elastic modulus due to irradiation for monolayer composites, although no significant modulus degradation was reported at lower irradiation doses of a few dpa [26]. On the other hand, no notable change or only a slight reduction (~20%) in elastic moduli was observed after HNS-ML for irradiation to 100 dpa.

Figures 5 and 6 summarize the dose dependences of PLS and UFS, respectively, for CVI SiC/SiC composites with different F/M interfaces. Flexural test results for HNS-ML in previous studies [39, 41,

42] were plotted together. Similar to the elastic modulus, the PLS and UFS of multilayer composites with a thick (>50 nm) innermost PyC layer—HNS-C/ML and SA3-C/ML in this study—were plotted as the same category of monolayer composites. Both PLS and UFS showed a tendency to decrease with increasing neutron dose. In particular, the largest degradation of strength in monolayer composites with HNS fibers was identified after irradiation to 11–44 dpa at 450–640°C. In contrast, mechanical degradation to the same dose level upon irradiation was obvious for SA3 composites, but the dose dependence was rather moderate (20–30 % of non-irradiated PLS and ~40 % of non-irradiated UFS) compared with the steep dose dependence of the HNS composites (15–50 % of non-irradiated PLS and 20–60 % of non-irradiated UFS).

(3) Microstructure and fracture surfaces

Figures 7 and 8 show typical flexural fracture surfaces of non-irradiated and neutron-irradiated SiC/SiC composites, respectively, with varied F/M interfaces. For non-irradiated composites, the fiber pullout length for SA3 composites (SA3-C and SA3-C/ML) was shorter than that for HNS composites (HNS-C and HNS-C/ML). The fractures thus look more fibrous in the HNS composites. In contrast, no clear differences was found in fracture appearance owing to the difference in the interface types tested in this study. Composites with both monolayer and multilayer interfaces show brush-like fractures with moderate fiber pullout. In the case of irradiation to 44 dpa at 590–640°C, there was no obvious change in macroscopic fracture appearance due to irradiation. Fiber pullout was always abundant, although the fiber pullout length was different depending on the fiber type. But microscopically, an indication of change was found in the fracture cross-section of the fiber, especially the HNS fiber: an obvious river pattern was seen in non-irradiated fibers, but it seemingly disappeared after irradiation. This result is consistent with the fracture surfaces of HNS fibers irradiated to 70~100 dpa in previous studies [39, 41]. No notable change in the cross-section for the SA3 fiber was seen.

Figure 9 shows typical SEM images of the open edges of each composite before and after irradiation. As clearly indicated in the images of irradiated composites, there are many pits at the fiber edges, especially for the HNS-fiber–reinforced composites (HNS-C and HNS-C/ML). Although both the HNS fiber and the CVI-SiC matrix were highly crystalline, a difference in the dimensional stability was identified. In Figure 9, pit depths of >10 μm can be seen. In contrast, no significant dimensional mismatch can be observed in the composites with SA3 fibers (SA3-C and SA3-C/ML), which show a comparatively flat surface.

Figure 10 shows typical SEM images of the cross-sections of each composite after irradiation. Regardless of the interface type, micro-cracking occurred at the F/M interface even before any mechanical testing. Note specifically that the cracks propagated near the fiber surface in the multilayer

composites. The other features were noted in SA3-fiber–reinforced composites; many pores were detected in the fiber centers of the irradiated material. In the high-magnification images in Fig. 11, such pores are not found in the non-irradiated SA3 fiber but are found in irradiated SA3 fiber. On the other hand, pore formations were not identified in the HNS fiber, as shown in Fig. 12. In contrast, carbon phases, which were further identified in non-irradiated fibers, remained unchanged after irradiation for both cases.

Figures 13–15 show high-resolution TEM images of the non-irradiated and neutron-irradiated F/M interfaces. In the non-irradiated SiC/SiC composites (Figs. 13 and 14), a layered structure was observed in the innermost PyC layer, and the layers appeared to be randomly oriented. This is a very common structure in PyC fabricated by the CVI method, showing the high fraction of sp^2 bond, i.e., graphitic structure [46]. The layered structure was more noticeable in the multilayer specimens. More importantly, it was found that the graphitic layers were lost in all the irradiated PyC; i.e., irradiation-induced amorphization of PyC occurred (Fig. 15). In contrast to the irradiated specimen images in Fig. 10, cracking was induced at the F/M interface by irradiation to 44 dpa at 590–640°C for all composite types, even without mechanical loading. High-resolution images in Fig. 15 also clearly identify cracking at the F/M interface of the HNS composite. A crack has penetrated into the PyC layer. No visible cracking was identified in the non-irradiated interfaces.

Discussion

(1) Strength stability following irradiation at intermediate irradiation temperatures

PLS is often considered to be the matrix cracking stress for ceramic-fiber–reinforced ceramic matrix composites, although the matrix cracking behavior is generally complicated and depends on fabric architecture, loading mode, and so on [47, 48]. Of many models, Evans and Vagaggini proposed a comprehensive model to forecast PLS from constituent properties [49, 50]. The model was originally developed for 1-dimensional (1D) composites for structural simplicity; but the underlying failure mechanism has been widely adopted in composite design, test, and simulation for not only 1D but also 2D and 3D composites [29, 51, 52]. The model indicates that PLS is affected by changes in the F/M interfacial properties and matrix toughness, rather than by the fiber strength itself. In this series of irradiation experiments, similar properties were considered for the CVI-SiC matrix before and after irradiation [26], so irradiation-induced F/M interfacial property changes were a key phenomenon. One of the causes of mechanical degradation of composites is degradation of the F/M interface, i.e., single crack penetration from matrix to fiber through the F/M interface, due to loss of carbon at the F/M interface—as was indicated in HNS-ML after irradiation to 70–100 dpa at 300°C [39, 41]. However, this mechanism was unlikely in this case because progressive fiber pullout was obvious from Fig. 8. Indeed, note that interfacial cracks were first identified in the irradiated composites before mechanical testing (Fig. 10).

Moderate interfacial debonding was associated with significant fiber pullout, resulting in quasi-ductility, as observed in HNS-ML irradiated to 70–100 dpa [39, 41]. However, an excessive loss of load-transferring capability at the F/M interface due to progressive fiber debonding simultaneously resulted in a significant reduction of PLS, based on the Evans and Vagaggini model [49, 50]. The interfacial deterioration (i.e., interfacial debonding) is therefore an explanation for the measured severe degradation of PLS in the monolayer composites in this study.

Curtin [53, 54] proposed a fracture strength model for the tensile loading of unidirectionally fiber-reinforced composites, and the model was extended and applied to flexure evaluation by McNulty et al. [55]. Both models clearly indicate the importance of the statistical strengths of SiC fibers, as well as of the F/M interfacial properties. It has been reported that single-filament tensile test results have demonstrated the superior strength retention of HNS and SA3 after irradiation to a few dpa (0.6~7.7 dpa) at irradiation temperatures of 280–800°C [56, 57]. However, the effects of irradiation to higher neutron doses are still uncertain, since no mechanical test data are presently available. As an alternative, fiber strength has been assessed by the fractography method. For instance, fracture mirror observations suggest possible deterioration of HNS fibers by irradiation to 70 dpa at irradiation temperatures of ~500°C [41]. The mirror radius has increased by the irradiation. It is well known that in brittle ceramics, the reciprocal fiber strength is proportional to the square root of the mirror radius [54]. In this study, Fig. 8 shows that irradiation changed the fracture surface appearances of the HNS fibers. The fracture mirror was measurable for the non-irradiated HNS fiber, but the overall part of the fracture surface of the irradiated fiber exhibited a mirror-like zone, i.e., indicative of an increase in the mirror radius due to irradiation. This implies probable degradation of fiber strength. In contrast, no significant change in the fracture surface of the SA3 fiber was observed. No clear mirror zone was identified before or after irradiation. One important observation was the formation of tiny pores inside the SA3 fiber (Fig. 11), which are potential origins of cracking. However, whether the formation of such pores has any impact on fiber strength is not clear. Therefore, fiber deterioration cannot be denied based on the limited information so far available. As an alternative, it is concluded that the most likely mechanism of the considerable degradation in fracture strength for all of the composites tested in this study that resulted from irradiation to 11–44 dpa at 450–640°C is interfacial deterioration (i.e., interfacial debonding).

In previous sections, it was clearly noted that the interfacial deterioration was a primary cause of mechanical degradation for SiC/SiC composites irradiated to 11–44 dpa at 450–640°C and understanding interfacial shear properties is therefore important. It is generally recognized that interfacial shear properties, including both interfacial debonding shear strength and interfacial friction stress, affect interfacial cracking and fiber pullout behavior. Both properties are generally determined by radial clamping stresses at the F/M interface, which are generally subject to thermal stress, irradiation-induced

stress, thermal and irradiation creep, roughness-induced stress, and Poisson expansion; and are closely related to the PyC interlayer thickness [32, 58–60]. Sauder et al. [61] evaluated the optimum F/M interface structure using the interfacial clamping model with consideration of the residual stresses induced at the F/M interface and fiber surface roughness in the absence of neutron irradiation. The model calculation estimated that the minimum thickness of a PyC interlayer is 30 nm for non-irradiated HNS composites and 60 nm for non-irradiated SA3 composites to maintain noncatastrophic failure with the moderate F/M interfacial role. In other words, the model explains that a thinner PyC layer results in robust clamping at the F/M interface. For instance, HNS-ML with very thin (<20 nm) PyC sequences shows comparatively higher interfacial shear properties due to the strong clamping effect of the rough surfaces of fibers, resulting in shorter fiber pullout [39, 41]. In a similar manner, monolayer composites also have the potential to retain equivalent load transfer if the PyC interface is sufficiently thin (~20 nm). For the HNS composite in our experiments, the PyC monolayer was 70–130 nm thick; the PyC interface of concern was comparably thick and undoubtedly preferable to maintain sufficient quasi-ductility in fracture for non-irradiated test conditions (Fig. 3). However, the roughness-induced stress of the monolayer composites used in this study must be lower than that of the HNS-ML in previous studies [39–42]. In contrast, for the SA3 composite with a PyC interlayer thickness of 50–130 nm, almost the same or a slightly larger thickness is needed to show the transition of change determined by ref. [61]. this feature (i.e., strong bonding at the F/M interface) can be clearly found from the fiber pullout appearance in Figs. 7 and 8. Typically, the surface roughness of SA3 fibers (~60 nm) is four times greater than that of HNS fiber (~15 nm) [61]. Thus, a more fibrous fracture was seen in the smoother HNS composites owing to lower clamping stress due to the fiber surface roughness.

Irradiation-induced stresses at the F/M interface are caused mainly by differential swelling of the composite constituents, i.e., the SiC fibers and the matrix. The PyC F/M interface is extremely important to retain structural stability, i.e., dimensional stability with good strength retention, during irradiation because the mechanical properties of composites are readily affected by residual stresses at the F/M interface. Structural instability caused by irradiation was observed in early-generation SiC/SiC composites, e.g., amorphous-based Nicalon SiC fiber–reinforced CVI-SiC matrix composites [22, 23]. Amorphous-based Nicalon shrinks during irradiation, while highly crystalline CVI-SiC swells. As a result of differential dimensional changes between Nicalon and CVI-SiC, interfacial cracking occurred as a result of irradiation-induced stress, resulting in brush-like fracture with progressive fiber debonding at the F/M interface. In contrast, structural stability has been much improved by selecting highly crystalline advanced SiC fibers, e.g., HNS and SA3 [22, 23]. The present study is, however, the first case in which, similar to early-generation composites, interfacial debonding occurred without any mechanical loading during heavy neutron irradiation to 44 dpa at intermediate irradiation temperatures. It is obvious from

Fig. 3 that the load transfer function was almost lost after fiber pullout only in irradiated monolayer composites, regardless of the fiber type. Crack initiation upon irradiation to 11 dpa at 500°C was also suspected, based on the post-irradiation flexural test data. An explanation is differential swelling between the fiber and the matrix, which was obvious for the HNS-fiber–reinforced composites in Fig. 9. Differential dimensional changes between fiber and matrix can cause residual stress at the F/M interface. However, once cracking occurs, the clamping stress must decrease further because of the reduced contribution from the roughness-induced stress in the SiC/SiC composites with a sufficiently thick (>50 nm) PyC interlayer in this study. Weaker clamping means poor load transfer at the F/M interface, which eventually causes a significant reduction in PLS and UFS. This strength reduction as a result of poor load transfer may have occurred in the HNS composites, but it cannot fully explain the initiation of interfacial cracking in the SA3 composites. It has been recognized that SA3 fiber is comparatively morphologically stable under ion irradiation, and similar ion-irradiation–induced swelling in SA3 fiber and a CVI-SiC matrix has hence been found [62].

Details of the neutron irradiation effects on the interfacial shear properties at the fiber and PyC interface, as well as between fiber and matrix, were evaluated [32]. The push-out method was applied to the thin-sliced composite cross-section, and an analytical model indicated interfacial debonding shear strength and interfacial friction stress as key interfacial shear parameters of the fiber/PyC interface. The former parameter is closely related to the cracking initiation event, and the latter is related to the load transfer during the fiber pullout process after fiber debonding. Both monolayers and multilayers were evaluated to ~7.7 dpa over an irradiation temperature range of 380–1080°C. Both interfacial debonding shear strength and interfacial friction stress decreased with increasing neutron dose at the beginning of irradiation and approached a constant value for each parameter. The saturation stress level was generally dependent on the PyC thickness; but in many cases, it was higher in the multilayer composites, which showed more than double the interfacial debonding shear strength of the monolayer composites (t_{PyC} = 520–720 nm in the [32]). Nevertheless, it must be recognized that the interfacial debonding shear strength for monolayer composites was still high enough to retain load transfer at the F/M interface after irradiation to ~7.7 dpa at an irradiation temperature range of 380–800°C, since no strength degradation was measured after that irradiation. Under these conditions, no cracking at the F/M interface was identified for the irradiated state.

For neutron irradiation to >10 dpa, Ozawa et al. [63] claimed that tensile hysteresis loop analysis of Tyranno-SA3/PyC/CVI-SiC composites irradiated to 12 dpa at 750°C found no degradation of sliding stress at the F/M interface, which is closely related to the interfacial debonding shear strength and interfacial friction stress [50, 64–66]. However, it must be recognized that the superior irradiation stability of the flexural strength of multilayer composites in this case was achieved because the PyC interlayer was

sufficiently thin (20–60 nm), similar to the HNS-ML case. In short, a comparatively large roughness-induced clamping stress was likely obtained even if the interface debonded during irradiation. The 4-phase cylinder model for evaluating residual radial stress [32] has shown that the residual radial stress becomes more negative, i.e., the clamping stress increases, with increasing fiber surface roughness and with decreasing PyC interlayer thickness. A fundamental question is therefore why the load transfer function at the F/M interface was drastically reduced by irradiation at 11–44 dpa only for the composites tested in this study and not for HNS-ML composites tested in previous studies. It is speculated that the irradiation-induced morphological change in comparatively thick PyC (t_{PyC} = 70–130 nm for HNS and t_{PyC} = 50–130 nm for SA3) at intermediate irradiation temperatures of ~600°C significantly affects the cracking resistance. The F/M interface was more subject to irradiation-induced residual stress rather than roughness-induced clamping stress for the comparatively thick PyC interface because the interlock effect schematically described in [61] might be lost with increasing PyC interface thickness. Such a thick PyC interphase no longer supported sufficient load transfer without roughness-induced clamping once it was cracked. In addition, the different swelling behaviors of PyC among this and previous studies might affect any cracking events that occur.

The elastic moduli of composites can generally be estimated by a rule of mixture [67, 68]. First, it is assumed that the fundamental irradiation behavior of the SiC matrix is similar for all composite types because both HNS and SA3 materials are high-purity polycrystalline beta SiC. The elastic modulus of CVD-SiC exhibits a dependence on irradiation temperature: the modulus decreases with decreasing irradiation temperature because of greater radiation-induced lattice expansion; the reduction in the elastic modulus was up to 6–11% for length changes of 0.29–0.53% at ~600°C [69]. This is common for any type of composite if the SiC constituents are highly crystalline and near-stoichiometric. From this point of view, the same magnitude of modulus reduction due to irradiation at lower irradiation temperatures (6–11%) is possible since both fiber (HNS and SA3) and matrix (CVI-SiC) are highly crystalline and near-stoichiometric. Indeed, relative elastic moduli exhibiting such reductions are found in refs. [26, 39, 41, 42]. Especially for multilayer composites, this trend agreed with the model prediction for CVD-SiC [45, 69]. Basically the same is true for monolayer composites, with the exception of the data obtained in this study. In contrast, the irradiation-assisted modulus change in the PyC itself contributed less to the overall change in the composite modulus, since the total fraction of PyC is 2–3% for both monolayer and multilayer composites when it is assumed that the fiber volume fraction is 0.3–0.4. Therefore, the modification of the elastic moduli of SiC and PyC materials induced only by irradiation cannot explain the 31–53% reduction in the elastic moduli. It was concluded that the main reason for that reduction is irradiation-enhanced fiber debonding at the F/M interface.

(2) Dimensional stability of SiC/SiC composites and SiC fibers irradiated at intermediate irradiation temperature

Swelling of composites is generally determined as a result of dimensional changes in the individual constituents, i.e., fiber, matrix, and F/M interface, and a mixture of these. However, the PyC was expected to contribute very little to the overall dimensional change in the composite resulting from the interface structural change, because the volume fraction of the PyC was very small (2–3%) regardless of the interface structure. Therefore, the major contributor to composite swelling was expected to be SiC.

It has been reported that swelling of SiC ceramics is insensitive to neutron doses beyond 1 dpa at <1000°C, and the saturated swelling level depends on irradiation temperature [45]. The key driver of swelling is mainly the accumulation of radiation-induced point defects and their clusters in SiC in this temperature range for high-purity crystalline SiC [45]. In this study, the quality of the SiC matrix formed by the CVI method was common to all composite types.

Kondo et al. estimated swelling of HNS and SA3 fibers irradiated to ~100 dpa by the ion irradiation technique, although the irradiation temperature of 300°C was lower than the temperatures with which we were concerned [62]. They evaluated the dimensional changes in the irradiated fiber cross-section, as well as in the matrix cross-section, and reported that the swelling of the SA3 fiber was equivalent to that of the CVI-SiC matrix. The demonstrated superior dimensional stability of SA3 fiber under high-dose irradiation in ref. [62] is consistent with the intermediate-temperature irradiation case, as inferred from the fact that there was no gap at the fiber/matrix boundary on the free edge of the as-machined SA3 composite specimen (Fig. 9). In contrast, irradiation-enhanced shrinkage of the HNS fiber irradiated to 100 dpa was noted in ref. [62]. If we assume the same dimensional changes along the specimen length and width directions, and complete fiber debonding at the F/M interface, the swelling of the HNS fiber can be estimated based on the step at the HNS fiber and matrix interface in Fig. 9. From Fig. 9, it is obvious that the minimum step height at the interface is approximately 10 μm, corresponding to a length change of the HNS fiber of −0.7% relative to the CVI SiC matrix—i.e., the HNS fiber probably shrank. Shrinkage of the HNS fiber affects the swelling of composites if the F/M interface is intact. However, irradiation-enhanced fiber debonding without any mechanical loading is obvious in Fig. 10. The macroscopic composite swelling can therefore be determined mainly by the SiC matrix in a case of interfacial debonding. Indeed, there was no clear differences in the swelling data for HNS and SA3 composites in Fig. 2, although some swelling mismatch between fiber and matrix was evident from Fig. 9 for the HNS composite cases.

(3) Future prospects for development of SiC/SiC composites for nuclear applications

This study clearly demonstrates that thinner PyC layers are preferable in nuclear applications. In particular, it is recognized that the interlock contribution at the F/M interface owing to fiber surface roughness plays an important role in the load transfer function, retaining quasi-ductility. For that purpose, the optimum PyC thickness needs to be explored based on the same approach used for non-irradiated SiC/SiC composites by Sauder et al. [61]. Specifically, future investigations should focus on interface optimization for SA3 composites for application temperatures around 500–600°C, since many deficiencies were evident for HNS composites. Presently the target thickness is <50 nm for SA3, as the minimum thickness of the innermost PyC of this study. It is also required to confirm the exact range by further irradiation experiments because of the lack of irradiation data. In parallel, further investigation of irradiation effects on PyC, including detailed microstructural analysis of as-processed PyC, would be very useful.

In contrast, there was some indication of degradation of both HNS and SA3, although careful evaluation with comprehensive understanding of the mechanism is strongly desired. For this aspect, high-dose irradiation data for fiber strength are lacking. Detailed fracture mirror analysis may help to estimate the remaining strength of fibers embedded in the matrix after irradiation. Also, separate single-filament tensile tests would be valuable to quantify the irradiation-induced changes in fiber strength, providing statistical data.

Conclusions

This study evaluated the effects of neutron irradiation on CVI SiC/SiC composites containing two types of fibers, HNS and SA3, and either monolayer or multilayer F/M interfaces. The study focused on the influences of high-dose neutron irradiation (11–44 dpa) at intermediate temperatures of 450–640°C. Flexural properties and fractography were evaluated, and the resulting data were compared with the mechanical test results of previous studies (conducted at ~100 dpa). The key findings are summarized as follows.

1) Mechanical properties of SiC/SiC composites strongly depended on the innermost PyC layer adjacent to the SiC fiber. SiC/SiC composites with a comparably thick (>50 nm) PyC interphase adjacent to the fiber, regardless of whether they were monolayer or multilayer, even if the first PyC layers had about the same thickness, experienced considerable strength degradation under high-dose neutron irradiation to 11–44 dpa at lower irradiation temperatures (450–640°C). However, SiC/SiC composites with thin PyC/SiC multilayers showed superior strength retention after irradiation at similar neutron dose and radiation temperature conditions.

2) Debonding at the F/M interface during irradiation to 44 dpa at 590–640°C was obvious for all composites with a comparatively thick innermost PyC interlayer. Interfacial deterioration was the main cause of a reduction in mechanical properties, i.e., elastic modulus, PLS, and UFS.
3) The interfacial debonding in HNS composites was attributed not only to PyC morphological change but also to the reduced swelling (or probable irradiation-assisted shrinkage) of the HNS fiber.
4) SA3 fiber irradiated to 44 dpa at 590–640°C was found to have higher dimensional stability than the HNS fiber, although it was found that micro-pores formed in the SA3 fiber centers after irradiation under the same conditions.
5) This study found that a thin multilayer PyC/SiC interface with a carbon thickness of ~20 nm exhibited superior irradiation resistance, in terms of retention of mechanical properties, to the other interface system with thicker PyC. This was the case for CVI SiC/SiC composites reinforced with HNS fibers irradiated to ~40 dpa at ~600°C, assuming an equivalent microstructure of the PyC. The increased roughness-induced clamping stress for a comparatively thin PyC layer enabled to good load transfer via the bonded F/M interface, resulting in good strength retention after neutron irradiation.

Acknowledgements

This research was sponsored by the Office of Fusion Energy Sciences, US Department of Energy, and QST under contracts DE-AC05-00OR22725 and NFE-10-02779, respectively, with UT-Battelle, LLC. A portion of this research used resources at the High Flux Isotope Reactor, a DOE Office of Science User Facility operated by Oak Ridge National Laboratory.

References

[1] T. Noda, Evaluation of transmutation and low induced radioactivity and requirements for candidate structural materials, J. Nucl. Mater. 233–237 (1996) 1475–1480.

[2] E.E. Bloom, The challenge of developing structural materials for fusion power systems, J. Nucl. Mater. 258–263 (1998) 7–17.

[3] S.J. Zinkle, N.M. Ghoniem, Operating temperature windows for fusion reactor structural materials, Fusion Eng. Des. 51–52 (2000) 55–71.

[4] M.S. Tillack, X.R. Wang, D. Navaei, H.H. Toudeshki, A.F. Rowcliffe, F. Najmabadi, ARIES Team, Design and analysis of the ARIES-ACT1 fusion power core, Fusion Sci. Technol. 67 (2015) 49–74.

[5] X.R. Wang, M.S. Tillack, C. Koehly, S. Malang, H.H. Toudeshki, F. Najmabadi, ARIES team, ARIES-ACT2 DCLL power core design and engineering, Fusion Sci. Technol. 67 (2015) 193–219.

[6] D. Maisonnier, I. Cook, S. Pierre, B. Lorenzo, D.P. Luigi, G. Luciano, N. Prachai, P. Aldo, DEMO and fusion power plant conceptual studies in Europe, Fusion Eng. Des. 81 (2006) 1123–1130.

[7] Y. Poitevin, M.A. Futterer, L. Giancarli, A.L. Puma, J.F. Salavy, J. Szczepanski, Status of the design and performances of the WCLL test blanket module for ITER-FEAT, Fusion Eng. Des. 61–62 (2002) 431–437.

[8] P. Sardain, D. Maisonnier, L. Di Pace, L. Giancarli, A.L. Puma, P. Norajitra, A. Orden, E. Arenaza, D. Ward, The European power plant conceptual study: Helium-cooled lithium-lead reactor concept, Fusion Eng. Des. 81 (2006) 2673–2678.

[9] G.O. Hayner, INEEL/EXT-03-01128 (2003).

[10] G.O. Hayner, INL/EXT 09-16547 (2008).

[11] K. Fitzgerald, D. Shepherd, Review of SiC_f/SiC_m corrosion, erosion and erosion-corrosion in high temperature helium relevant to GFR conditions, J. Nucl. Mater. 498 (2017) 476–494.

[12] C. Deck, G. Jacobsen, J. Sheeder, O. Gutierrez, J. Zhang, J. Stone, H. Khalifa, C. Back, Characterization of SiC-SiC composites for accident tolerant fuel cladding, J. Nucl. Mater. 466 (2015) 667–681.

[13] K. Yueh, K.A. Terrani, Silicon carbide composite for light water reactor fuel assembly applications, J. Nucl. Mater. 448 (2014) 380–388.

[14] D. Kim, H.-G. Lee, J.Y. Park, W.-J. Kim, Fabrication and measurement of hoop strength of SiC triplex tube for nuclear fuel cladding applications, J. Nucl. Mater. 458 (2015) 29–36.

[15] S.Y. Park, K.I. Ahn, Comparative analysis of station blackout accident progression in typical PWR, BWR, and PHWR, Nucl. Engng. Technol. 44 (2012) 311–322.

[16] V. Angelici Avincola, M. Grosse, U. Stegmaier, M. Steinbrueck, H.J. Seifert, Oxidation at high temperatures in steam atmosphere and quench of silicon carbide composites for nuclear application, Nucl. Engng. Des. 295 (2015) 468–478.

[17] Y. Kee, H.S. Kim, H.C. No, Failure probabilities of SiC clad fuel during a LOCA in public acceptable simple SMR (PASS), Nucl. Engng. Des. 292 (2015) 1–16.

[18] R.J. Price, Properties of silicon carbide for nuclear fuel particle coatings, Nucl. Technol. 35 (1977) 320–336.

[19] M. Takeda, J. Sakamoto, A. Saeki, Y. Imai, H. Ichikawa, High performance silicon carbide fiber Hi-Nicalon for ceramic matrix composites, Ceram. Eng. Sci. Proc. 16 (1995) 37–44.

[20] T. Ishikawa, Y. Kohtoku, K. Kumagawa, T. Yamamura, T. Nagasawa, High-strength alkali-resistant sintered SiC fibre stable to 2,200 °C, Nature 391 (1998) 773–775.

[21] Y. Xu, A. Zangvil, J. Lipowitz, J.A. Rabe, G.A. Zank, Microstructure and microchemistry of polymer-derived crystalline SiC fibers, J. Am. Ceram. Soc. 76 (1993) 3034–3040.

[22] L.L. Snead, Y. Katoh, A. Kohyama, J.L. Bailey, N.L. Vaughn, R.A. Lowden, Evaluation of neutron irradiated near-stoichiometric silicon carbide fiber composites, J. Nucl. Mater. 283–287 (2000) 551–555.

[23] T. Hinoki, L.L. Snead, Y. Katoh, A. Hasegawa, T. Nozawa, A. Kohyama, The effect of high dose/high temperature irradiation on high purity fibers and their silicon carbide composites, J. Nucl. Mater. 307–311 (2002) 1157–1162.

[24] K. Ozawa, Y. Katoh, T. Nozawa, L.L. Snead, Effect of neutron irradiation on fracture resistance of advanced SiC/SiC composites, J. Nucl. Mater. 417 (2011) 411–415.

[25] Y. Katoh, K. Ozawa, T. Hinoki, Y. Choi, L.L. Snead, A. Hasegawa, Mechanical properties of advanced SiC fiber composites irradiated at very high temperatures, J. Nucl. Mater. 417 (2011) 416–420.

[26] Y. Katoh, K. Ozawa, C. Shih, T. Nozawa, R.J. Shinavski, A. Hasegawa, L.L. Snead, Continuous SiC fiber, CVI SiC matrix composites for nuclear applications: Properties and irradiation effects, J. Nucl. Mater. 448 (2014) 448–476.

[27] T. Koyanagi, K. Ozawa, T. Hinoki, K. Shimoda, Y. Katoh, Effects of neutron irradiation on mechanical properties of silicon carbide composites fabricated by nano-infiltration and transient eutectic-phase process, J. Nucl. Mater. 448 (2014) 478–486.

[28] Y. Katoh, L.L. Snead, T. Cheng, C. Shih, W. Daniel Lewis, T. Koyanagi, T. Hinoki, C.H. Henager, Jr., M. Ferraris, Radiation-tolerant joining technologies for silicon carbide ceramics and composites, J. Nucl. Mater. 448 (2014) 497–511.

[29] R.R. Naslain, The design of the fiber-matrix interfacial zone in ceramic matrix composites, Compos. A 29 (1998) 1145–1155.

[30] R.R. Naslain, R. J.-F. Pailler, J. Lamon, Single- and multilayered interphases in SiC/SiC composites exposed to severe environmental conditions: an overview, Int. J. Appl. Ceram. Technol. 7 (2010) 263–275.

[31] S. Jacques, A. Lopez-Marure, C. Vincent, H. Vincent, J. Bouix, SiC/SiC minicomposites with structure-graded BN interphases, J. Eur. Ceram. Soc. 20 (2000) 1929–1938.

[32] T. Nozawa, Y. Katoh, L.L. Snead, The effect of neutron irradiation on the fiber/matrix interphase of silicon carbide composites, J. Nucl. Mater. 384 (2009) 195–211.

[33] CEGA, Report CEGA-002820, Rev 1 (July 1993).

[34] J.L. Kaae, The mechanical behavior of BISO-coated fuel perticles during irradiation. Part 1: analysis of stresses and strains generated in the coatuing of a BISO fuel particle during irradiation, Nucl. Technol. 35 (1977) 359–367.

[35] J.L. Kaae, Effect of irradiation on the mechanical properties of isotropic pyrolytic carbons, J. Nucl. Mater. 46 (1973) 121–133.

[36] J.L. Kaae, D.W. Stevens, J.C. Bokros, Dimensional changes induced in poorly crystalline isotropic carbons by irradiation, Carbon 10 (1972) 561–570.

[37] J.L. Kaae, J.C. Bokros, Irradiation-induced dimensional changes and ceep of isotropic carbon, Carbon 9 (1971) 111–122.

[38] Yu.S. Virgil'ev, I.G. Lebedev, Effect of neutron irradiation on properties of glassy carbon, Inorg. Mater 38 (2002) 668–673.

[39] T. Koyanagi, T. Nozawa, Y. Katoh, L.L. Snead, Mechanical property degradation of high crystalline SiC fiber-reinforced SiC matrix composite neutron irradiated to ~100 displacements per atom, J. Eur. Ceram. Soc. 38 (2018) 1087–1094.

[40] A.G. Perez-Bergquist, T. Nozawa, C. Shih, K.J. Leonard, L.L. Snead, Y. Katoh, High-dose neutron irradiation of Hi-Nicalon Type-S silicon carbide composites. Part 1: Microstructural evaluations, J. Nucl. Mater. 462 (2015) 443–449.

[41] Y. Katoh, T. Nozawa, C. Shih, K. Ozawa, T. Koyanagi, W. Porter, L.L. Snead, High-dose neutron irradiation of Hi-Nicalon Type-S silicon carbide composites. Part 2: Mechanical and physical properties, J. Nucl. Mater. 462 (2015) 450–457.

[42] G. Newsome, L.L. Snead, T. Hinoki, Y. Katoh, D. Peters, Evaluation of neutron irradiated silicon carbide and silicon carbide composites, J. Nucl. Mater. 371 (2007) 76–89.

[43] L. Filipuzzi, G. Camus, R. Naslain, Oxidation mechanisms and kinetics of 1D-SiC/C/SiC composite materials: I, an experimental approach, J. Am. Ceram. Soc. 77 (1994) 459–466.

[44] A.A. Campbell, W.D. Porter, Y. Katoh, L.L. Snead, Method for analyzing passive silicon carbide thermometry with a continuous dilatometer to determine irradiation temperature, Nucl. Instrum. Methods Phys. Res. B 370 (2016) 49–58.

[45] Y. Katoh, T. Koyanagi, J.L. McDuffee, L.L. Snead, K. Yueh, Dimensional stability and anisotropy of SiC and SiC-based composites in transition swelling regime, J. Nucl. Mater. 499 (2018) 471–479.

[46] J.Y. Yan, C.W. Chen, P.C. Fang, K.M. Yin, F.R. Chen, Y. Katoh, A. Kohyama, J.J. Kai, The investigation of crack mechanism for Tyranno-SA SiC/SiC composites with ESI method, J. Nucl. Mater. 329–333 (2004) 513–517.

[47] C. Cady, F. E. Heredia, A.G. Evans, In-plane mechanical properties of several ceramic-matrix composites, J. Am. Ceram. Soc. 78 (1995) 2065–2078.

[48] G.N. Morscher, Stress-de-endent matrix cracking in 2D woven SiC-fiber reinforced melt-infiltrated SiC matrix composites, Compos. Sci. Technol. 64 (2004) 1311–1319.

[49] A.G. Evans, F.W. Zok, Review the physics and mechanics of fibre-reinforced brittle matrix composites, J. Mater. Soc. 29 (1994) 3857–3896.

[50] E. Vagaggini, J.-M. Domergue, A.G. Evans, Relationship between hysterisis mesurements and the constituent properties of ceramic matrix composites: I, theory, J. Am. Ceram. Soc. 78 (1995) 2709–2720.

[51] T. Ogasawara, T. Ishikawa, H. Ito, N. Watanabe, I.J. Davies, Multiple cracking and tensile behavior for an orthogonal 3-D woven Si-Ti-C-O fiber/Si-Ti-C-O matrix composite, J. Am. Ceram. Soc. 84 (2001) 1565–1574.

[52] J. Lamon, A micromechanics-based approach to the mechanical behavior of brittle-matrix composites, Compos. Sci. Technol. 61 (2001) 2259–2272.

[53] W.A. Curtin, Theory of mechanical properties of ceramic-matrix composites, J. Am. Ceram. Soc. 74 (1991) 2837–2845.

[54] W.A. Curtin, In situ fiber strengths in ceramic-matrix composites from fracture mirrors, J. Am. Ceram. Soc. 77 (1994) 1075–1078.

[55] J.C. McNulty, F.W. Zok, Application of weakest-link fracture statistics to fiber-reinforced ceramic-matrix composites, J. Am. Ceram. Soc. 80 (1997) 1535–1543.

[56] Y. Katoh, L.L. Snead, T. Nozawa, S. Kondo, J.T. Busby, Thermophysical and mechanical properties of near-stoichiometric fiber CVI SiC/SiC composites after neutron irradiation at elevated temperatures, J. Nucl. Mater. 403 (2010) 48–61.

[57] T. Nozawa, T. Hinoki, L.L. Snead, Y. Katoh, A. Kohyama, Neutron irradiation effects on high-crystallinity and near-stoichiometry SiC fibers and their composites, J. Nucl. Mater. 329–333 (2004) 544–548.

[58] A. Agbossou, J. Pastor, Thermal stresses and thermal expansion coefficients of n-layered fiber-reinforced composites, Compos. Sci. Technol. 57 (1997) 249–260.

[59] H. Walther, On mathematical models for calculating the mechanical behaviour of coated fuel particles, Nucl. Eng. Design 18 (1972) 11–39.

[60] T. Iyoku, M. Ishihara, H. Shirai, Development of thermal/irradiation stress analytical code "VIENUS" for HTTR graphite block, J. Nucl. Sci. Technol. 28 (1991) 921–931.

[61] C. Sauder, A. Brusson, J. Lamon, Influence of interface characteristics on the mechanical properties of Hi-Nicalon type-S or Tyranno-SA3 fiber-reinforced SiC/SiC minicomposites, Int. J. Appl. Ceram. Technol. 7 (2010) 291–303.

[62] S. Kondo, T. Hinoki, M. Nonaka, K. Ozawa, Irradiation-induced shrinkage of highly crystalline SiC fibers, Acta Mater. 83 (2015) 1–9.

[63] K. Ozawa, T. Nozawa, Y. Katoh, T. Hinoki, A. Kohyama, Mechanical properties of advanced SiC/SiC composites after neutron irradiation, J. Nucl. Mater. 367-370 (2007) 713-718.

[64] A.G. Evans, J.-M. Domergue, E. Vagaggini, Methodology for relating the tensile constitutive behavior of ceramic-matrix composites to constituent properties, J. Am. Ceram. Soc. 77 (1994) 1425–1435.

[65] J.-M. Domergue, E. Vagaggini, A.G. Evans, Relationship between hysterisis mesurements and the constituent properties of ceramic matrix composites: II, experimental studies on unidirectional materials, J. Am. Ceram. Soc. 78 (1995) 2721–2731.

[66] J.-M. Domergue, F.E. Heredia, A.G. Evans, Hysteresis loops and the inelastic deformation of 0/90 ceramic matrix composites, J. Am. Ceram. Soc. 79 (1996) 161–170.

[67] Z. Hashin, Analysis of properties of fiber composites with anisotropic constituents, J. Appl. Mech. 46 (1979) 543–550.

[68] T. Ishikawa, K. Bansaku, N. Watanabe, Y. Nomura, M. Shibuya, T. Hirokawa, Experimental stress/strain behavior of SiC-matrix composites reinforced with Si-Ti-C-O fibers and estimation of matrix elastic modulus, Compos. Sci. Technol. 58 (1998) 51–63.

[69] L.L. Snead, T. Nozawa, Y. Katoh, T.-S. Byun, S. Kondo, D.A. Petti, Handbook of SiC properties for fuel performance modeling, J. Nucl. Mater. 371 (2007) 329–377.

List of tables

List of figures

Fig. 14 Typical TEM micrographs of the PyC interphase for non-irradiated SiC/SiC composites: (a) HNS-C, (b) HNS-C/ML, (c) SA3-C, and (d) SA3-C/ML.

Fig. 15 Typical TEM micrographs of the PyC interphase for neutron-irradiated (44 dpa at 590–640°C) SiC/SiC composites: (a) HNS-C, (b) HNS-C/ML, (c) SA3-C, and (d) SA3-C/ML.

Table 1 Key specifications of the SiC/SiC composites studied.

Material ID	HNS-C	HNS-C/ML	SA3-C	SA3-C/ML
Fiber	Hi-Nicalon Type-S Plain weave (P/W)	Hi-Nicalon Type-S Satin weave (S/W)	Tyranno-SA3 Plain weave (P/W)	Tyranno-SA3 Plain weave (P/W)
Matrix	CVI-SiC	CVI-SiC	CVI-SiC	CVI-SiC
Fiber/matrix (F/M) interface	80–120 nm PyC	70–130 nm PyC + ML*	50–80 nm PyC	100–130 nm PyC + ML*
Density [g/cm^3]	2.41	2.47	2.48	2.56
Fiber volume fraction [%]	37	53	40	44
Porosity [%]	22	20	20	18

*ML: (~100 nm SiC + ~20 nm PyC) × 4

Table 2 Results of post-irradiation evaluation of SiC/SiC composites with varied F/M interfaces. Note that numbers in parentheses indicate one standard deviation.

Materials	Neutron dose [dpa]	Irradiation temperature, T_{irr} [°C]	Length change [%]	Dynamic Young's modulus [GPa]	Flexural tangent modulus [GPa]	Proportional limit stress [MPa]	Ultimate flexural strength [MPa]
HNS-S	Non-irradiated		n/a	214 (30)	170 (68)	253 (94)	363 (170)
	11	500	0.40 (0.00)	139 (19)	94 (21)	124 (33)	171 (38)
	12	450	0.45 (0.01)	148 (6)	n/d	n/d	n/d
	44	590–640	0.32 (0.04)	106 (7)	81 (7)	40 (4)	88 (16)
HNS-C/ML	Non-irradiated		n/a	240 (9)	214 (25)	345 (118)	380 (114)
	11	500	0.34 (0.04)	152 (4)	96 (4)	147 (33)	272 (27)
	12	450	0.46 (0.03)	143 (12)	n/d	n/d	n/d
	44	590–640	0.29 (0.17)	150 (11)	104 (10)	45 (13)	83 (18)
SA3-C	Non-irradiated		n/a	252 (26)	170 (20)	287 (39)	463 (66)
	11	500	0.53 (0.03)	163 (9)	93 (9)	97 (18)	206 (3)
	12	450	0.47 (0.02)	158 (16)	n/d	n/d	n/d
	44	590–640	0.41 (0.10)	142 (12)	112 (17)	77 (19)	195 (19)
SA3-C/ML	Non-irradiated		n/a	227 (19)	174 (11)	267 (53)	425 (111)
	11	500	0.41 (0.04)	107 (18)	64 (6)	77 (26)	154 (21)
	12	450	0.48 (0.03)	121 (14)	n/d	n/d	n/d
	44	590–640	0.39 (0.14)	119 (13)	81 (6)	48 (29)	160 (22)

*n/a: not applicable, n/d: no data (not tested)

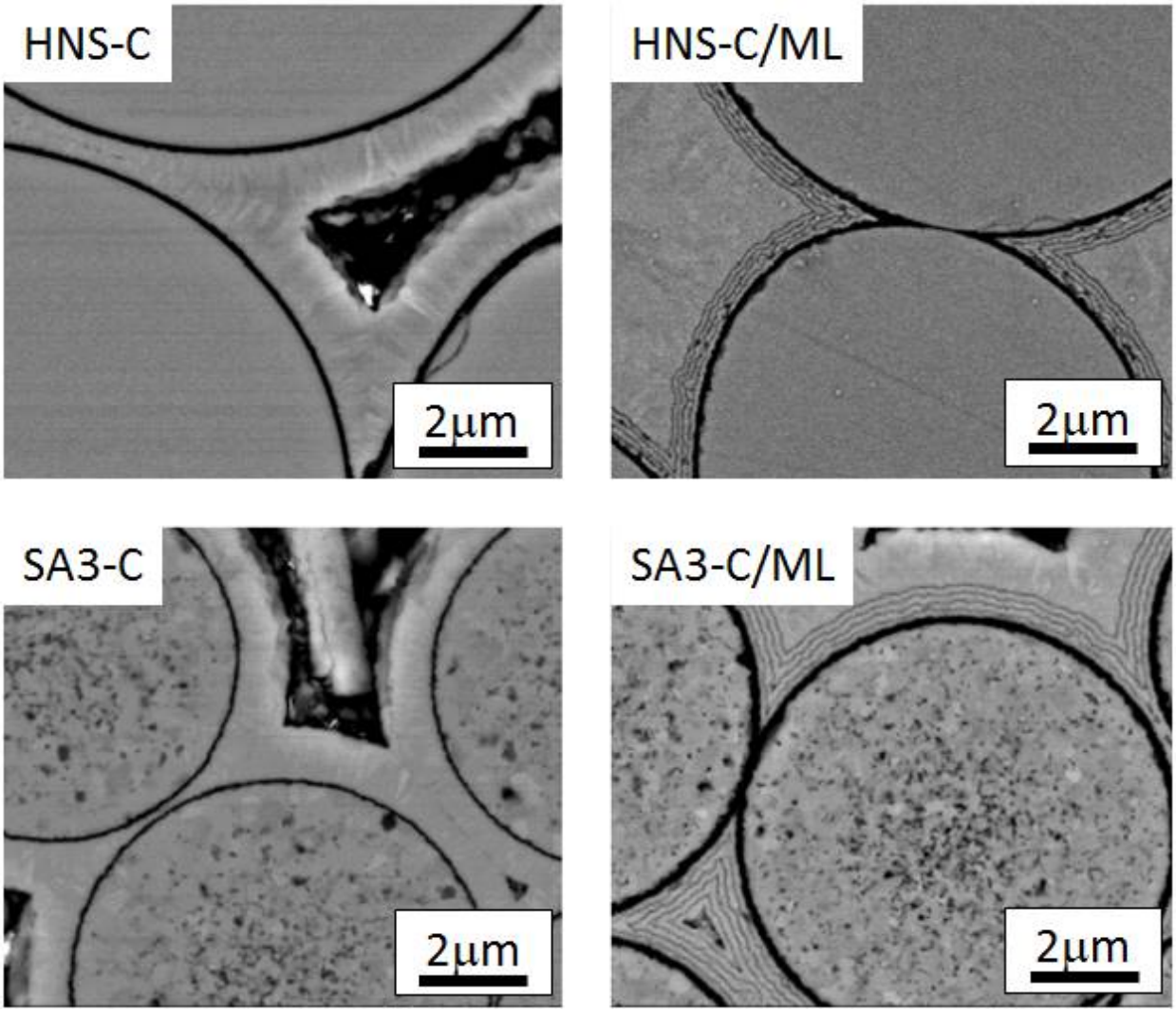

Fig. 1 Typical cross-sectional images of SiC/SiC composites tested.

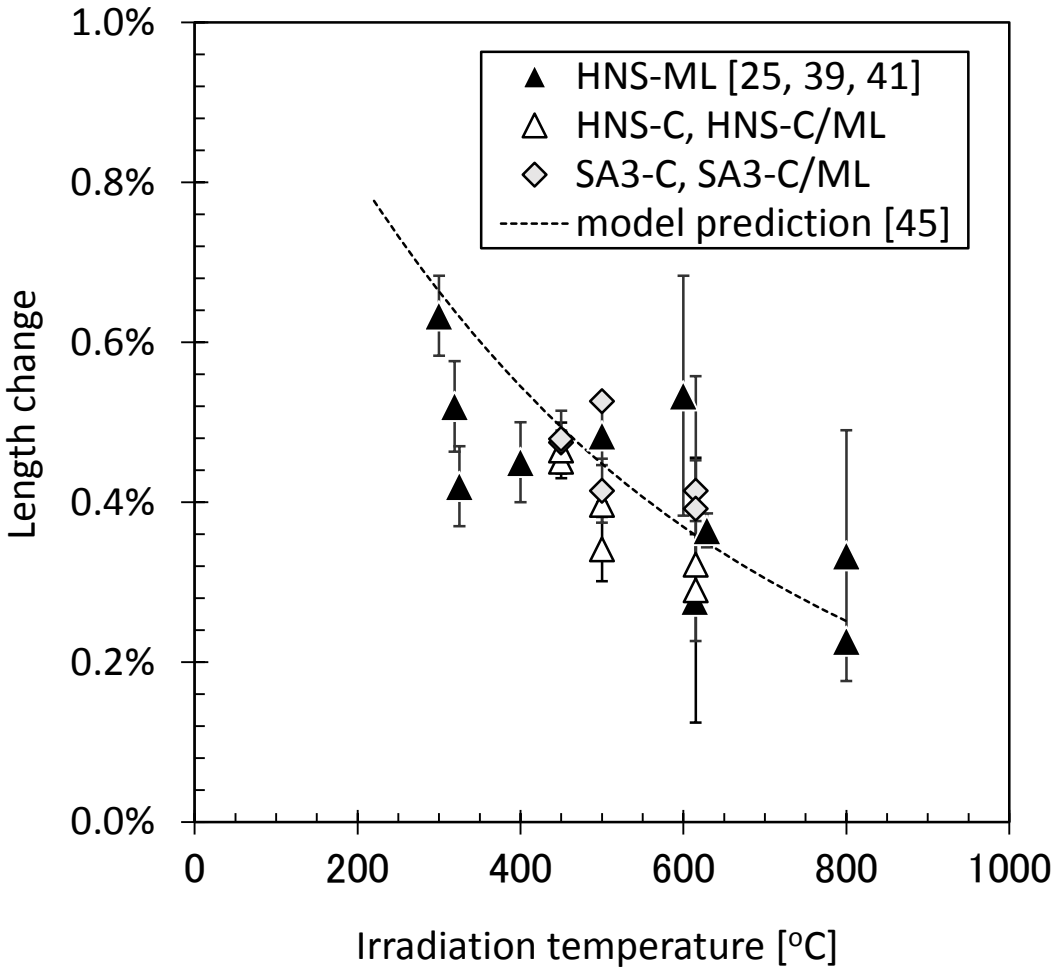

Fig. 2 Summary of length change of SiC/SiC composites. Error bars indicate ±1 standard deviation. The length changes predicted by the empirical model of Katoh et al. [45] are also plotted, shown as broken lines indicating irradiation temperature dependence.

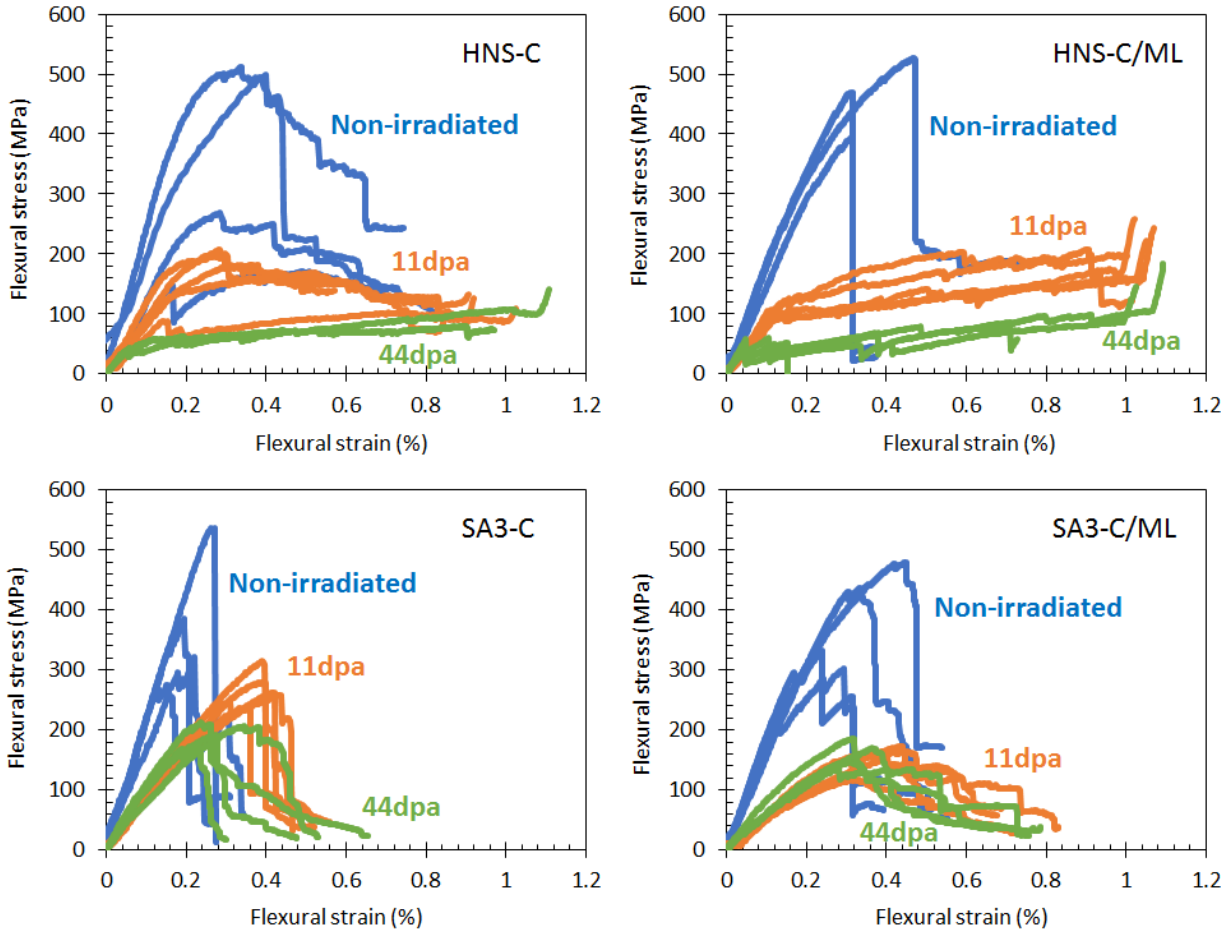

Fig. 3 Typical flexural behavior of non-irradiated and neutron-irradiated (11 dpa at 500°C and 44 dpa at 590–640°C) SiC/SiC composites with varied F/M interfaces.

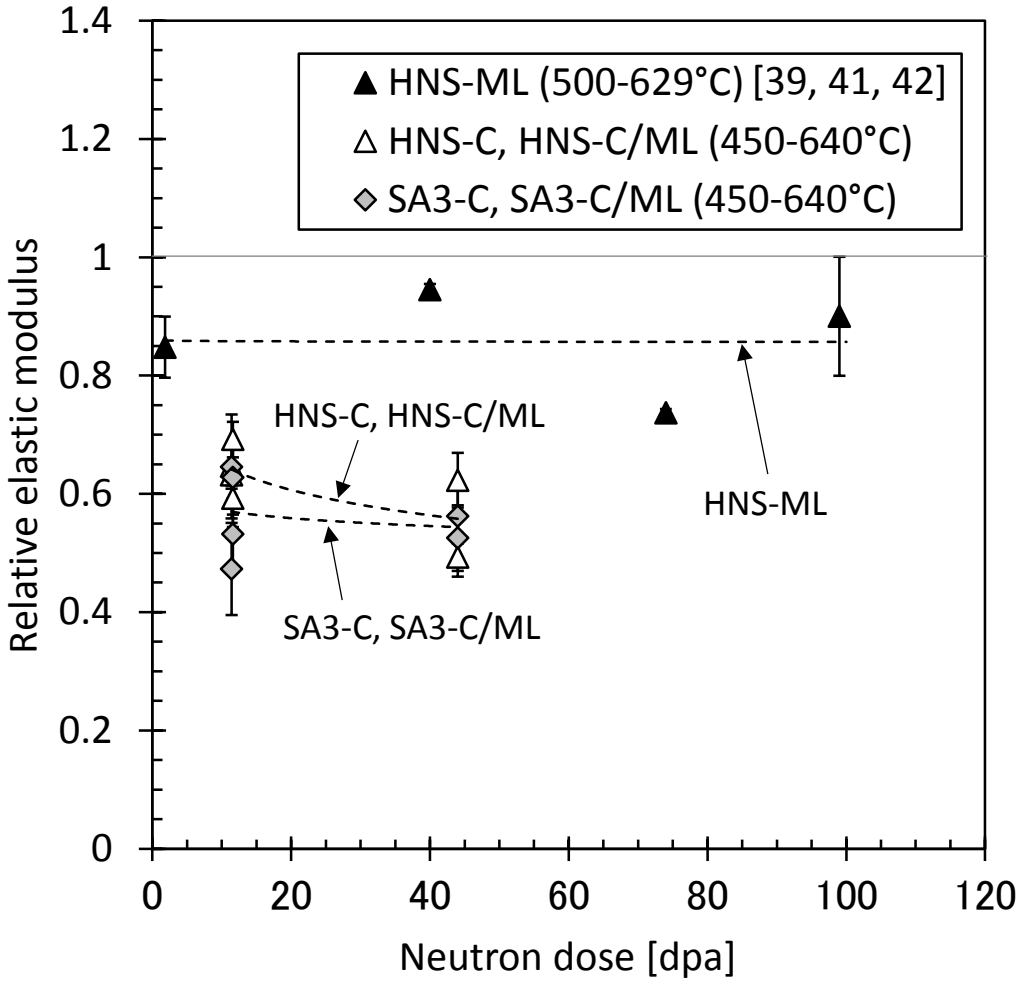

Fig. 4 Effect of neutron dose on elastic moduli of SiC/SiC composites with varied F/M interfaces. Error bars indicate ±1 standard deviation.

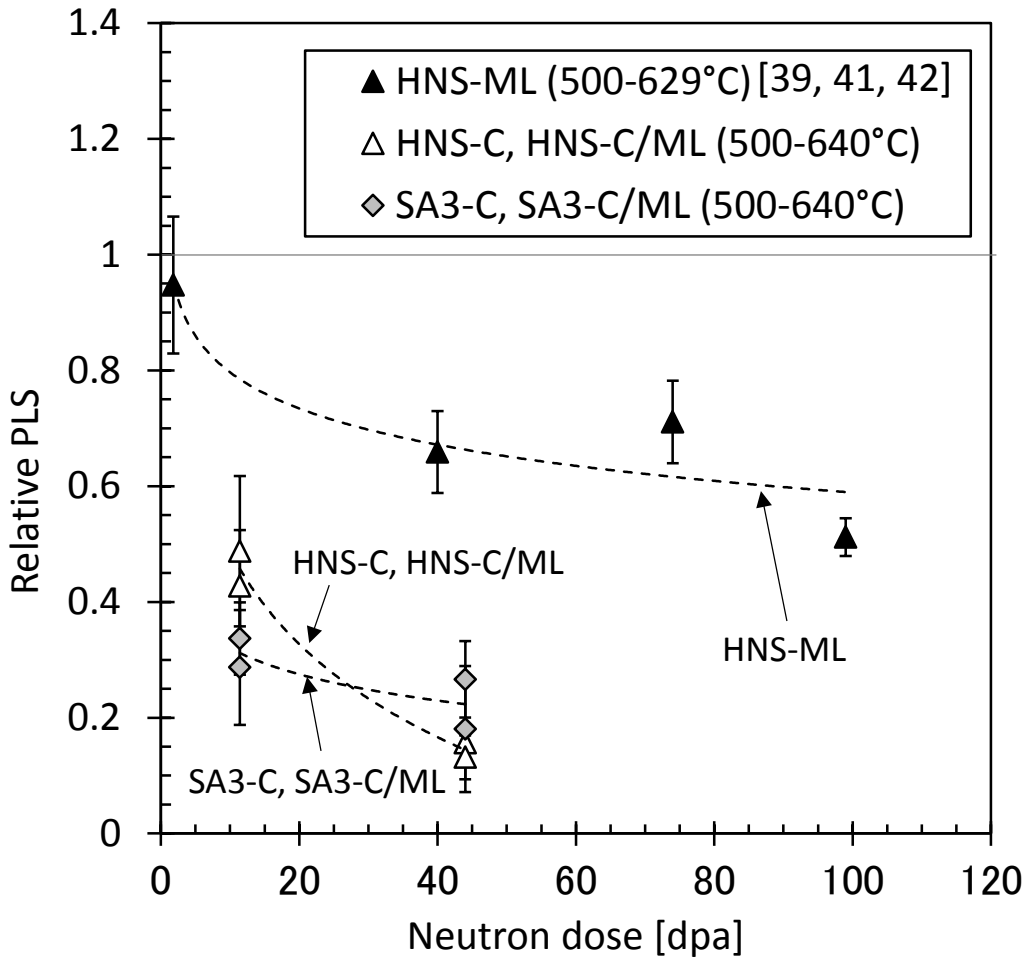

Fig. 5 Summary of neutron irradiation effects on proportional limit stress of SiC/SiC composites with varied F/M interfaces. Error bars indicate ±1 standard deviation.

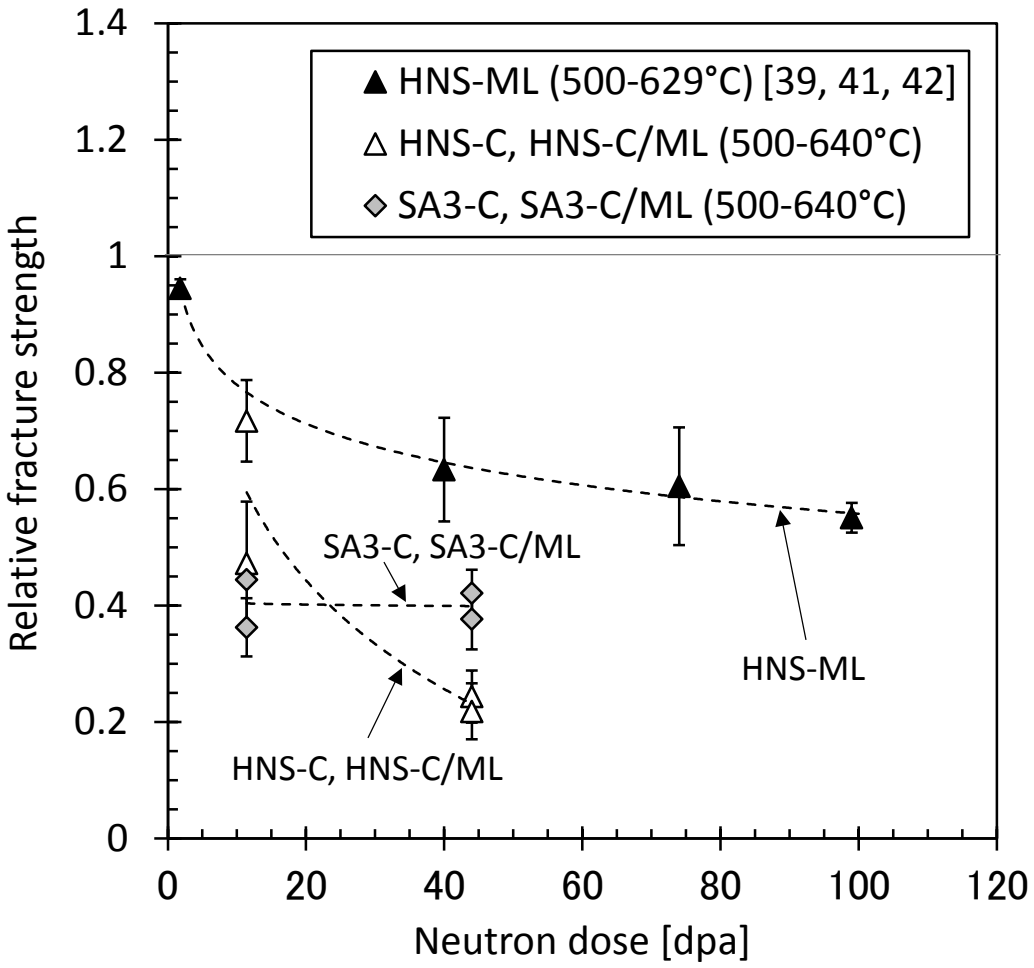

Fig. 6 Summary of neutron irradiation effects on fracture strength of SiC/SiC composites with varied F/M interfaces. Error bars indicate ±1 standard deviation.

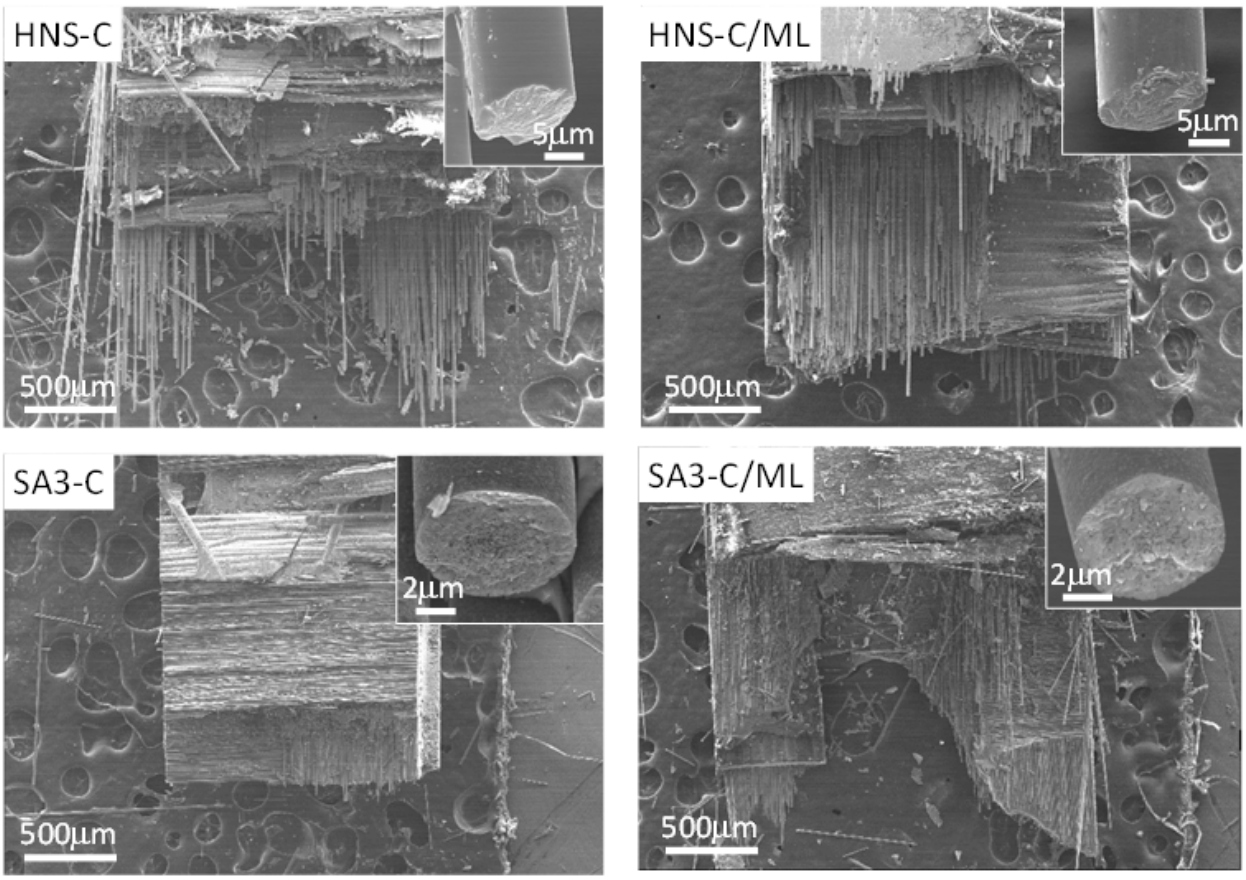

Fig. 7 Typical fracture surface appearance of non-irradiated SiC/SiC composites.

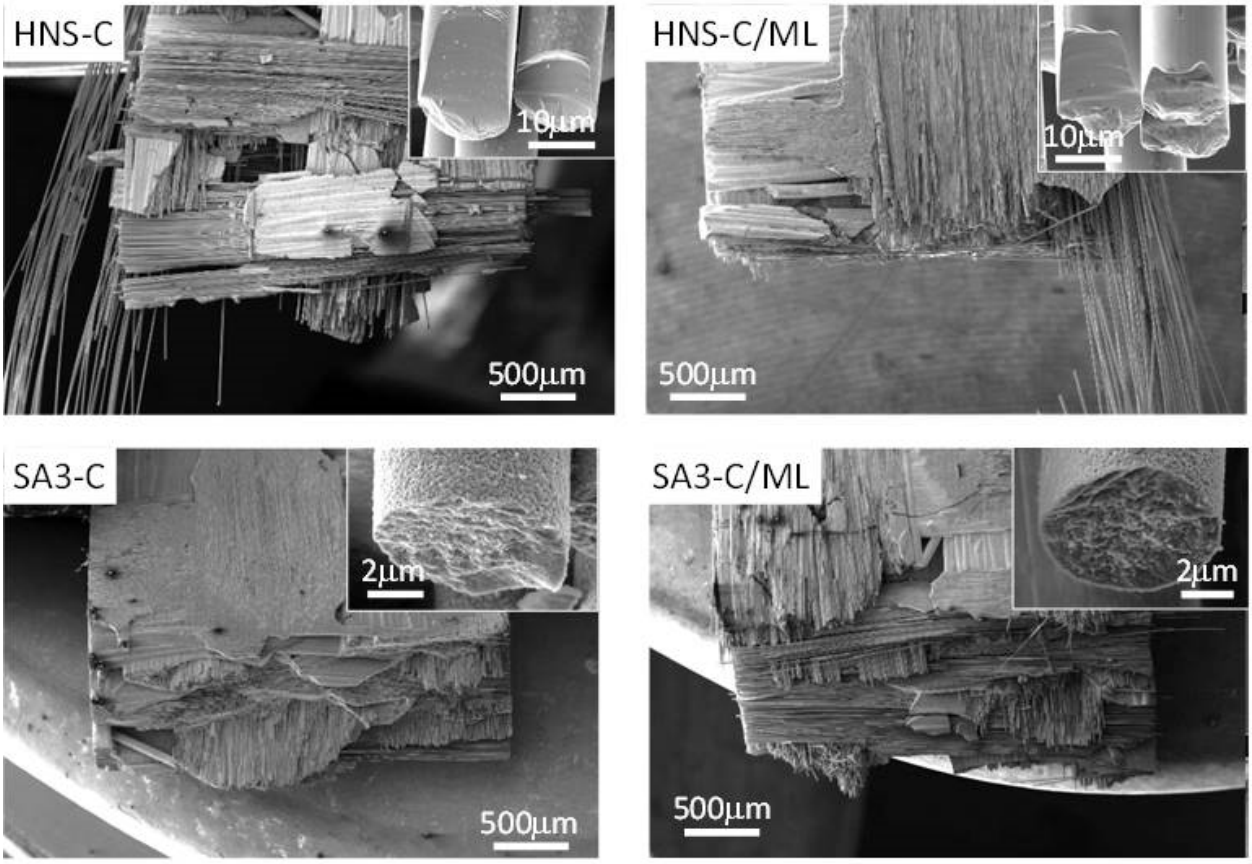

Fig. 8 Typical fracture surface appearance of SiC/SiC composites after neutron irradiation at intermediate temperatures (44 dpa at 590–640°C).

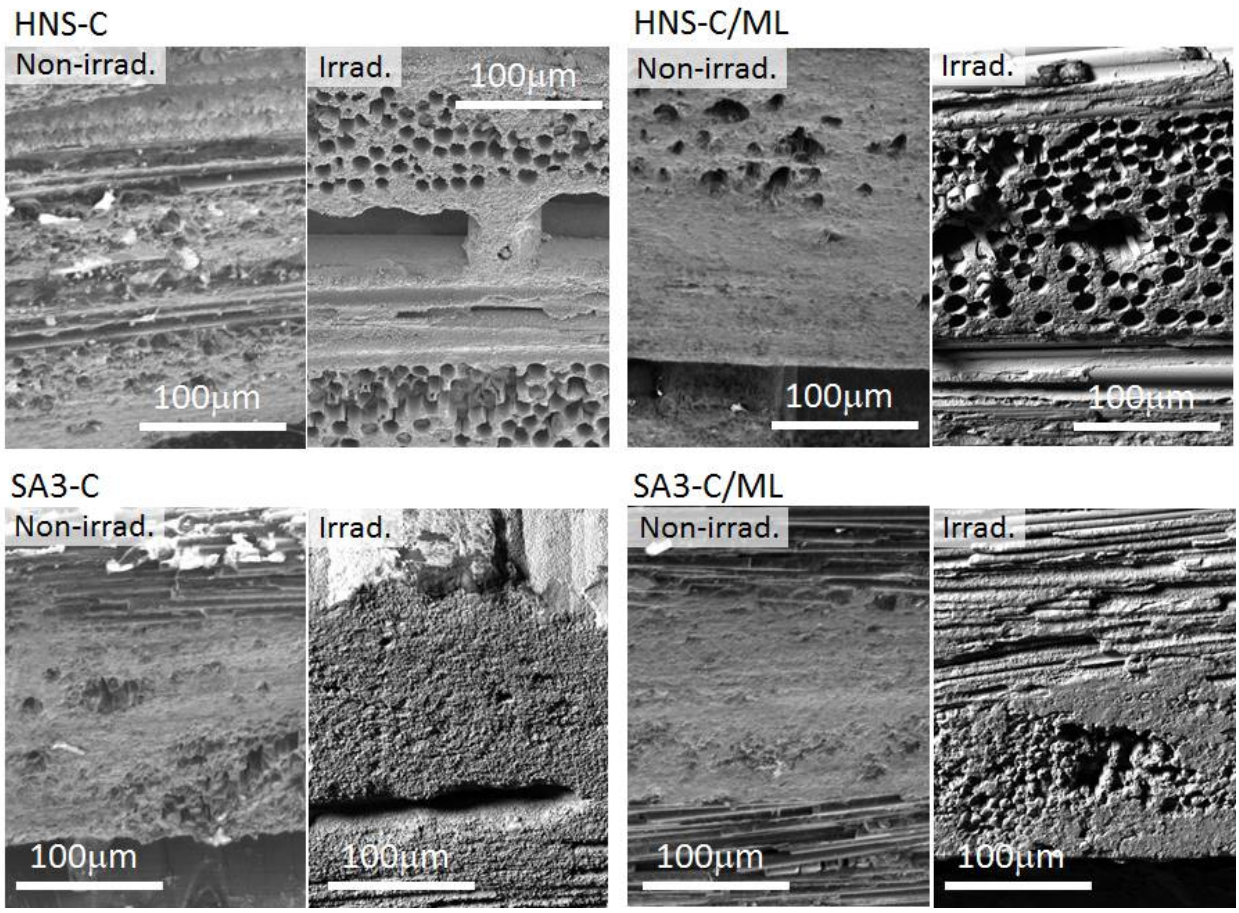

Fig. 9 Typical specimen edge images of SiC/SiC composites with varied SiC fibers and F/M interfaces before and after neutron irradiation (44 dpa at 590–640°C). Pores indicate greater matrix swelling than swelling of the fibers, resulting in recession of the fibers relative to the matrix.

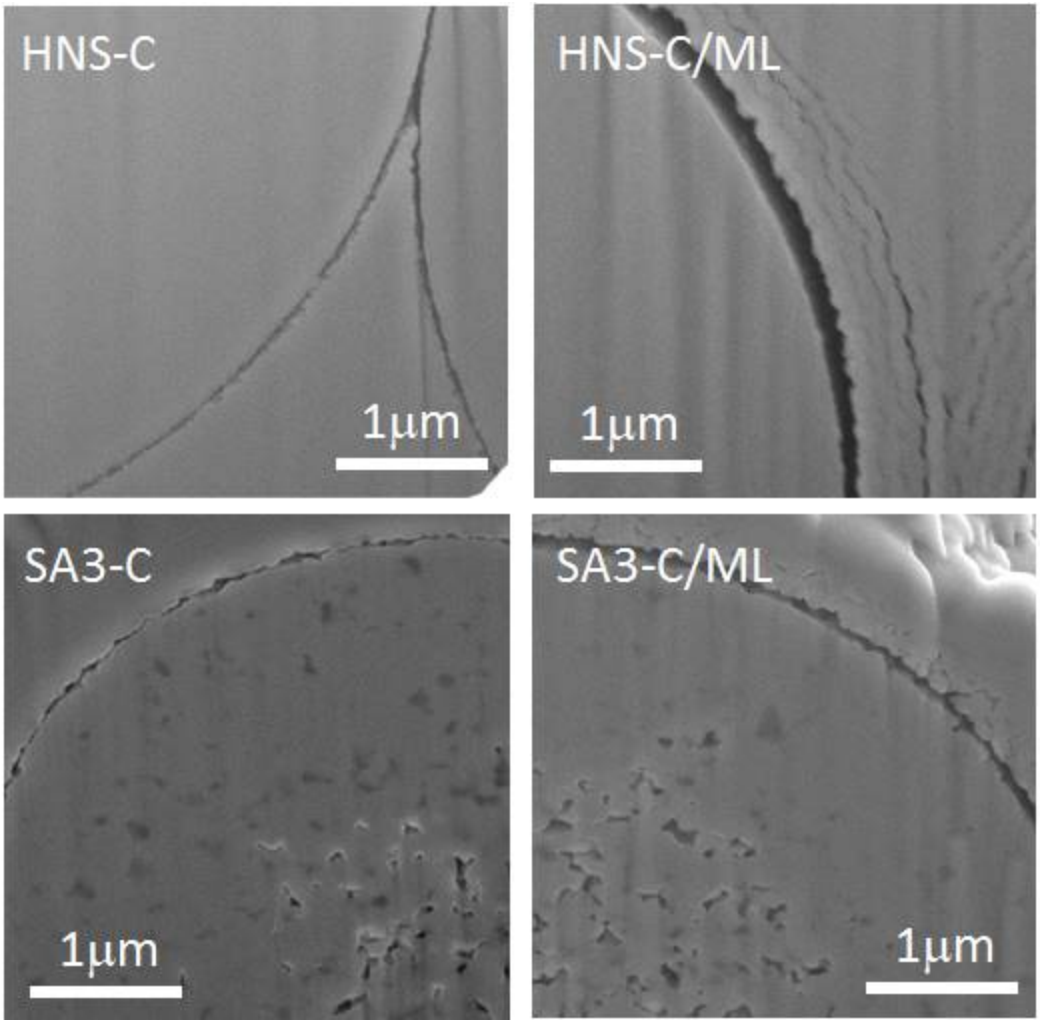

Fig. 10 Typical cross-sectional images of neutron-irradiated SiC/SiC composites with various SiC fibers and F/M interfaces (44 dpa at 590–640°C).

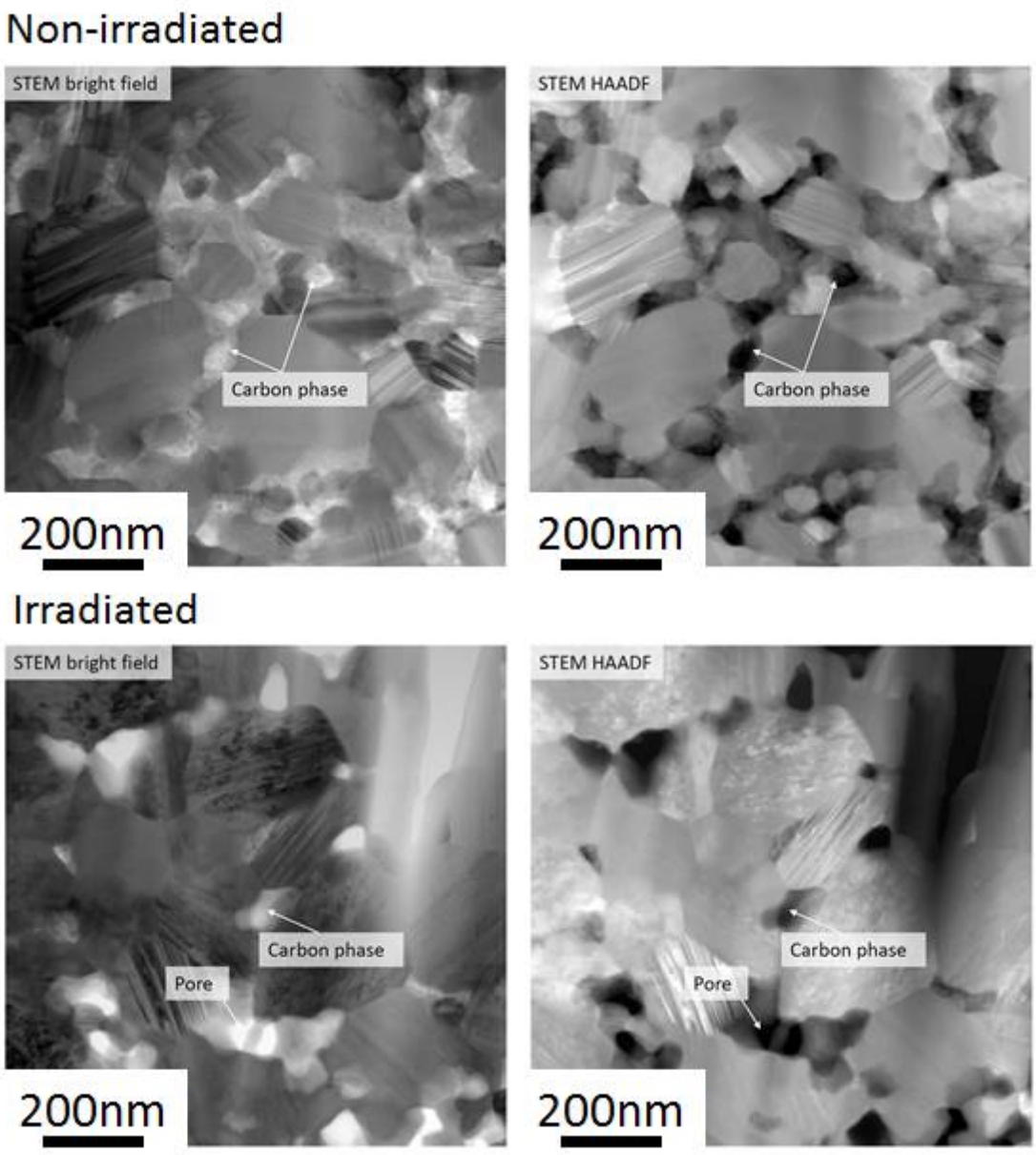

Fig. 11 Typical TEM micrographs of SA3 fiber before and after neutron irradiation (44 dpa at 590–640°C).

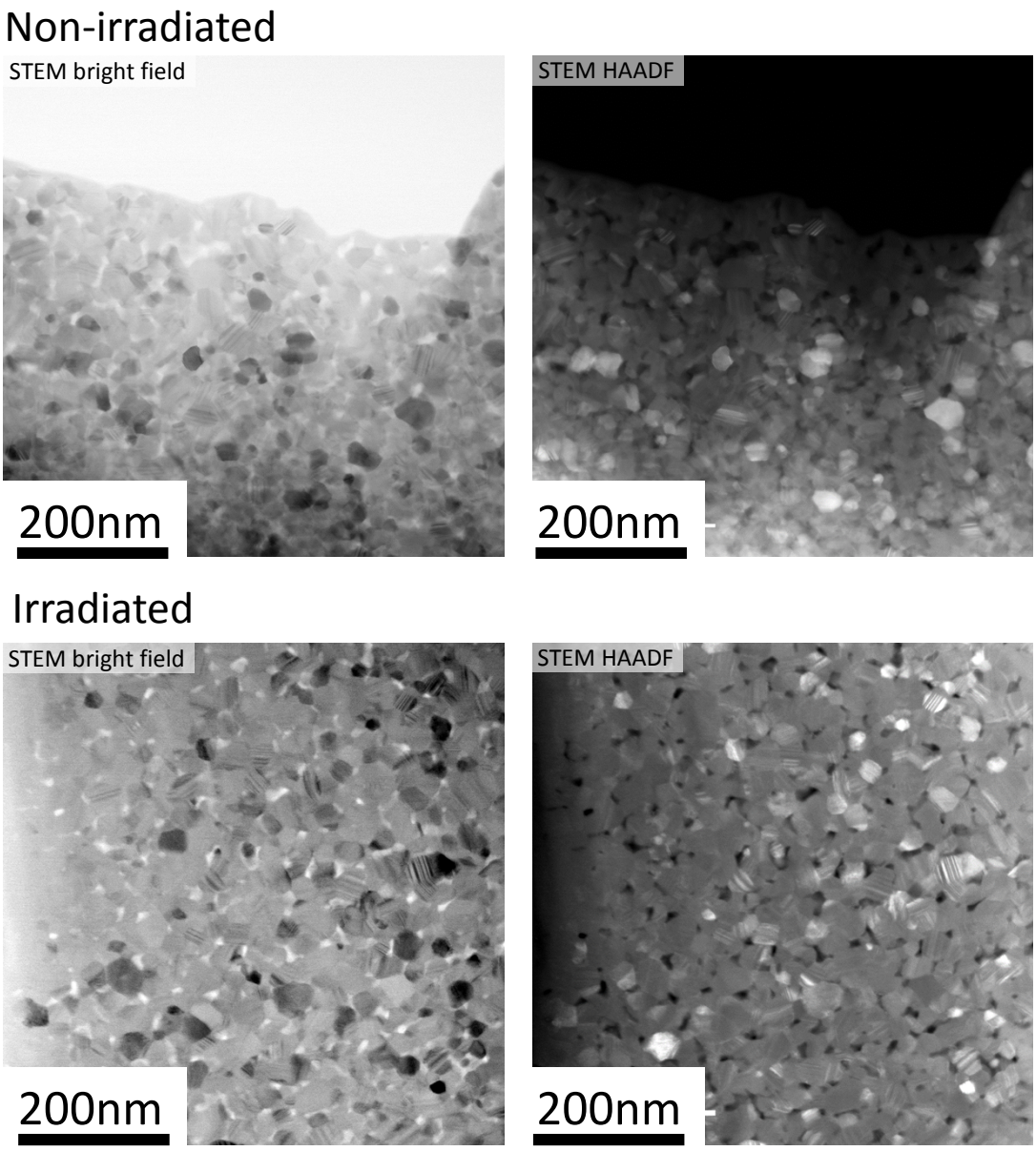

Fig. 12 Typical TEM micrographs of HNS fiber before and after neutron irradiation (44 dpa at 590–640°C).

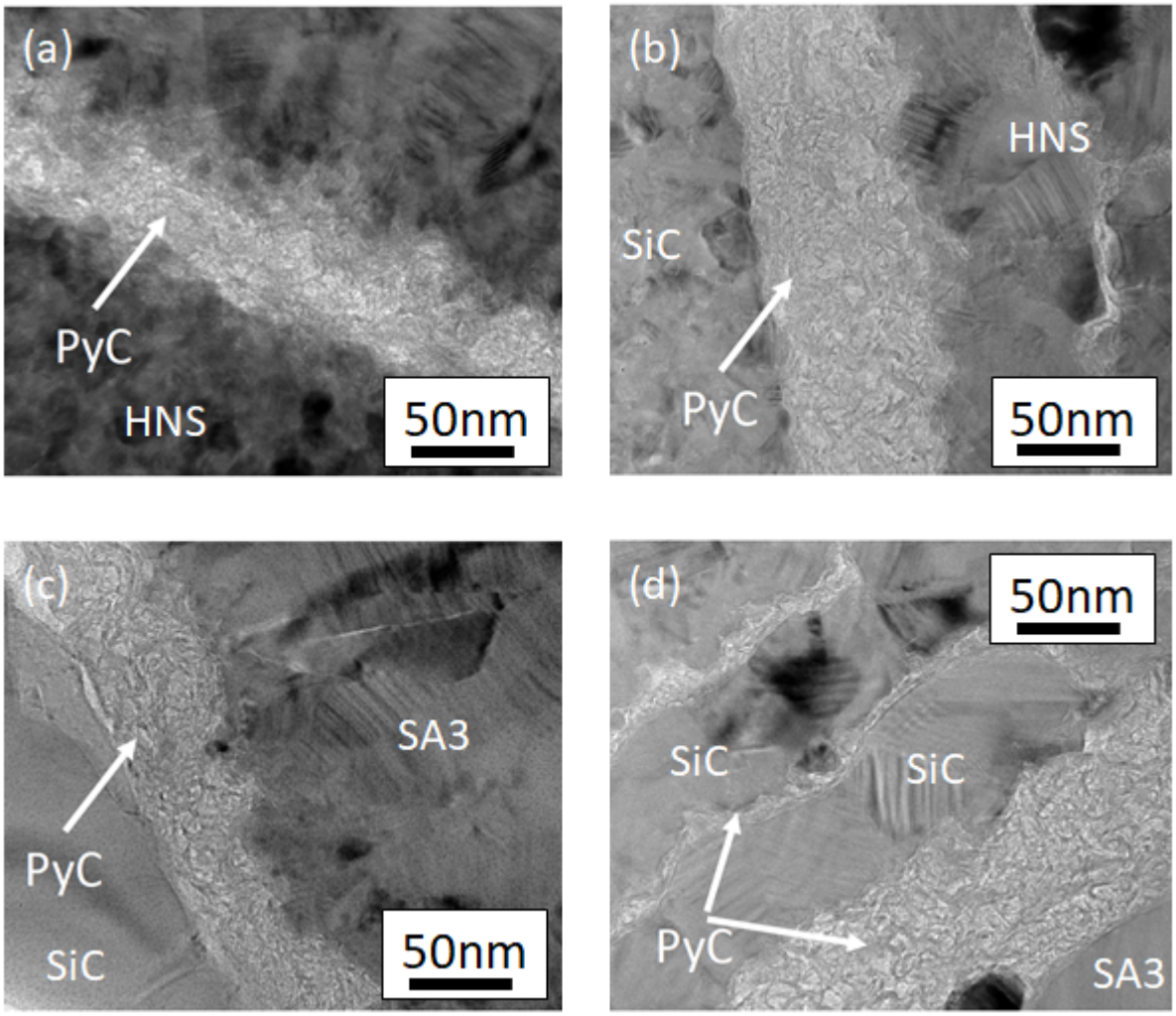

Fig. 13 Typical TEM micrographs of the F/M interface for non-irradiated SiC/SiC composites: (a) HNS-C, (b) HNS-C/ML, (c) SA3-C, and (d) SA3-C/ML.

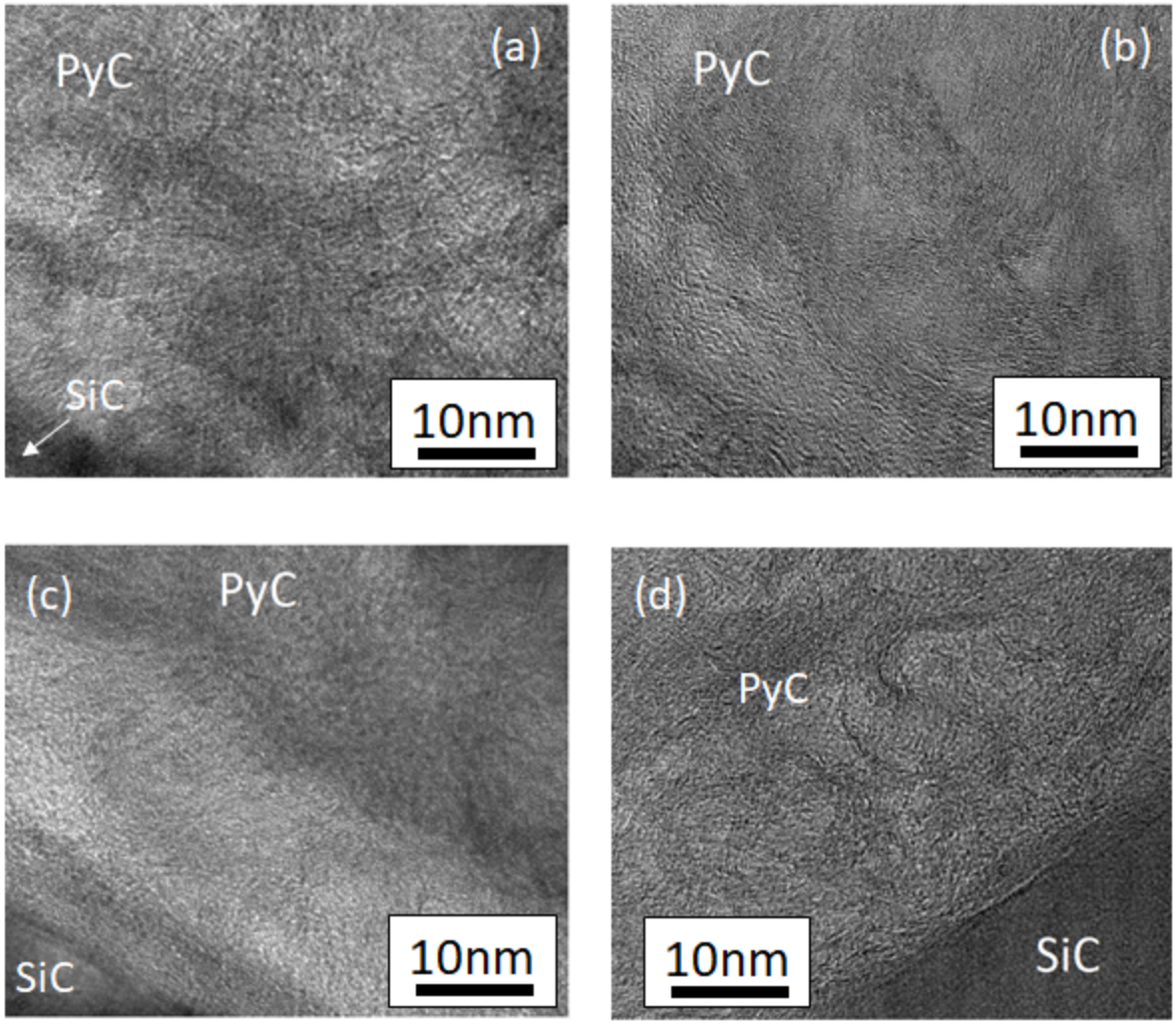

Fig. 14 Typical TEM micrographs of the PyC interphase for non-irradiated SiC/SiC composites: (a) HNS-C, (b) HNS-C/ML, (c) SA3-C, and (d) SA3-C/ML.

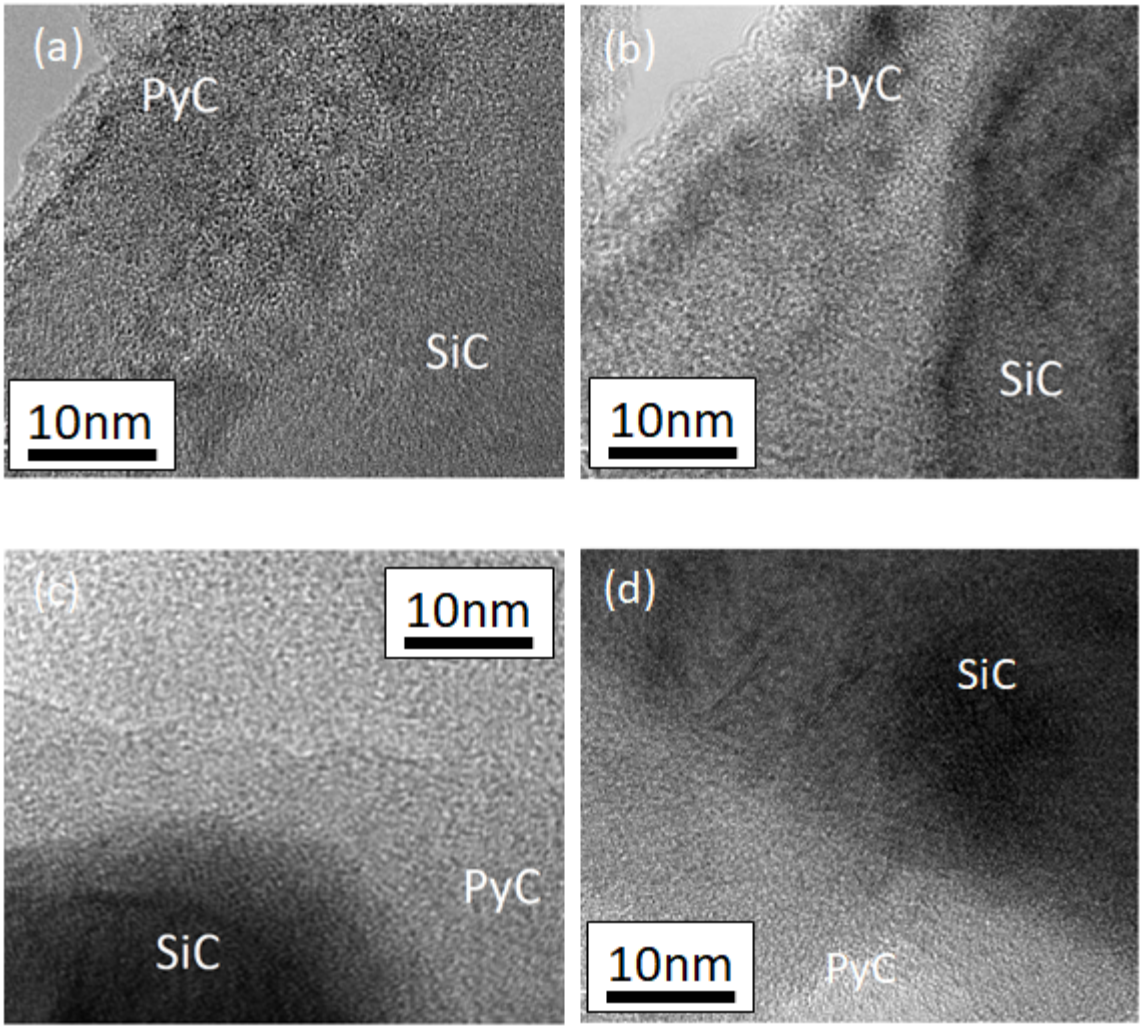

Fig. 15 Typical TEM micrographs of the PyC interphase for neutron-irradiated (44 dpa at 590–640°C) SiC/SiC composites: (a) HNS-C, (b) HNS-C/ML, (c) SA3-C, and (d) SA3-C/ML.